BRL

AD

MEMORANDUM REPORT NO. 1840

OPTICAL METHOD FOR ANALYSIS OF
ATMOSPHERIC EFFECTS ON LASER BEAMS

by

Paul H. Deitz

July 1967

Distribution of this document is unlimited.

U. S. ARMY MATERIEL COMMAND
BALLISTIC RESEARCH LABORATORIES
ABERDEEN PROVING GROUND, MARYLAND
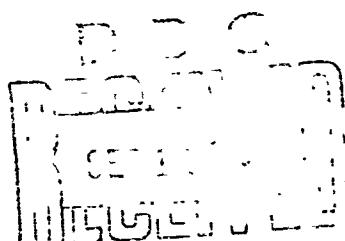
CLEARINGHOUSE

U.S. ARMY BALLISTIC RESEARCH LABORATORIES
ABERDEEN PROVING GROUND, MARYLAND

6 April 1967

ERRATA SHEET

for

BRL Memorandum Report No. 1840 entitled "Optical Method for Analysis of
Atmospheric Effects on Laser Beams", dated July 1967.

1. Page 16, line 9.   Change 5.0 to 0.50

2. Page 18, change the following entries in Table II to read:

	σ	C_n (calculated)
Afternoon	0.38	$2.0 \times 10^{-7} \ m^{-1/3}$
Night	0.14	$7.5 \times 10^{-8} \ m^{-1/3}$

3. Appendix - Re Figures A-1 to A-4, A-14: The photographs of the beam
    cross section should be oriented to show the step wedge along the
    left margin rather than the bottom margin. See text (pages 12-13)
    for optical system description.

BALLISTIC RESEARCH LABORATORIES

OPTICAL METHOD FOR ANALYSIS OF
ATMOSPHERIC EFFECTS ON LASER BEAMS

Paul H. Deitz

Ballistic Measurements Laboratory

ABERDEEN PROVING GROUND, MARYLAND

BALLISTIC RESEARCH LABORATORIES

MEMORANDUM REPORT NO. 1840

PHDeitz/sjw
Aberdeen Proving Ground, Md.
July 1967

OPTICAL METHOD FOR ANALYSIS OF
ATMOSPHERIC EFFECTS ON LASER BEAMS

ABSTRACT

This report describes the design of an instrumentation system for
the study of the effects of atmospheric turbulence on a collimated laser
beam under near-earth conditions.

The instrumentation consists of a helium-neon laser with optical
collimator and a receiving system of 24-inch aperture with narrow band-
pass filter.

The Appendix presents examples of beam cross section patterns for
different propagation conditions. The method of analyzing spatial
intensity distributions of these patterns is described.

3

TABLE OF CONTENTS

LIST OF FIGURES

7

LIST OF FIGURES (Continued)

Page

INTRODUCTION

Nearly all optical systems involve the transmission of electromagnetic radiation through an atmosphere. For most systems operating in controlled atmospheres, the medium is assumed to be homogeneous and its effect on system performance negligible. However, for long paths through the atmosphere the medium is not homogeneous and the index of refraction varies along the beam; this variation can be characterized statistically. Because of the effect of the medium on the transmitted beams, the performance of many optical systems is finally limited by atmospheric conditions.

To study these effects, the Ballistic Research Laboratories (BRL) have designed and built a high resolution, high stability optical receiving system. It is designed specifically for the study of light propagation in the near-earth atmosphere. A schematic drawing of the system is shown in Figure 1. This report describes the design of the system and the method used to analyze atmospheric effects on a collimated light beam recorded by the system. Results of the analysis show that the effects correlate well with those predicted by Tatarski.[1]* This system should be a valuable aid to a better understanding of atmospheric effects on optical systems.
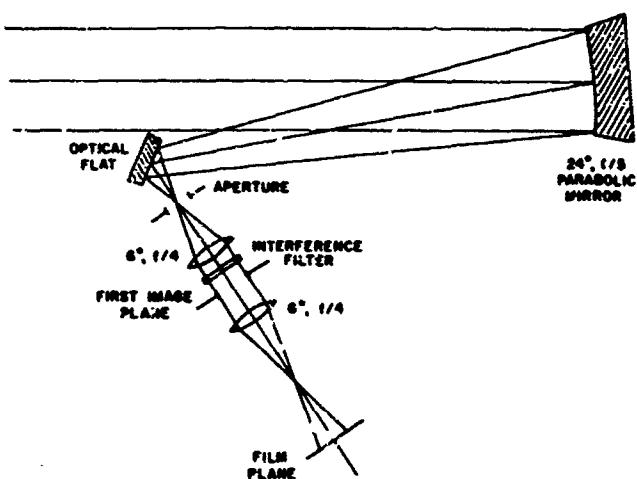

Figure 1. Ray diagram of optical receiver

INSTRUMENTATION

The light source is a helium-neon laser with a power of 10-milliwatts. The output can be attenuated by a polaroid filter and monitored at the laser. The attenuated beam is sent into a collimator with a spatial filter located at the focus of the eyepiece to remove intensity variations across the laser beam. The 2-inch objective lens is defocused slightly so that the transmitted Airy disc is somewhat larger than the receiver aperture at the range of 549 meters. The laser and related optics are held on an aimable mount. This system is located in a small trailer, solidly ground supported.

The optical system is contained in a 25-foot trailer making possible easy transportation from one site to another. On location, the heavily reinforced van is jacked free from its wheels. Inside the trailer, the optical system is mounted on an 8-inch I-beam frame. This frame is lifted free of the trailer floor by means of a three-point jacking system supported directly on the ground.

Collimated light impinging on a parabolic mirror 2 feet in diameter with a 10-foot focal length is reflected off-axis toward a plane mirror and then a focus. An aperture is placed at this focus which restricts the acceptance angle of the system to about two tenths of a degree. Next, an $f/4$, 6-inch focal length lens is placed one focal length from the aperture. Thus, the emerging light is collimated, making possible introduction of an interference filter which eliminates nearly all of any remaining background illumination. Beyond this first lens and filter is an image of the spatial intensity distribution at the 2-foot parabolic mirror. Alongside this image, an illuminated step wedge is projected in conjunction with fiducial lights to enable frame-to-frame correlation between a timed series of photographs. Both the intensity distributions of the parabolic mirror and the step wedge then are imaged by a second lens to a sensor plane at a magnification compatible with a chosen format.

10

CALIBRATION

An electromagnetic wave is completely characterized by its amplitude and phase. The optical receiver was set up to record the amplitude of the impinging radiation in terms of its related intensity. A 35-millimeter motion picture camera was placed in the film plane of the receiver to record the spatial intensity pattern of the incident radiation along with the calibrated step wedge. The wedge was calibrated at the film plane to an accuracy of 5 percent. The intensity variation across the extent of the entrance aperture of the receiver was measured by illuminating the parabolic mirror with the far-field pattern and scanning the image plane. Over the central 18 inches of the mirror, the intensity variation was less than 6 percent. A geometrical distortion and resolution test was made by placing a test screen in front of the receiver and back-illuminating it with the divergent laser beam. A grid array of holes on 10-centimeter centers was drilled in the board of such size as to give a 2 millimeter diameter Fraunhofer diffraction pat. on the parabolic mirror surface. Pictures were taken of this pattern and measured to a 1-micron precision on a comparator. Accurate measurements were made of the grid array, and a least squares fit computer program was run on these data. The standard deviation of the position of the image points related to object space and compared with the grid array was 0.7 millimeter with a resolution of 0.25 millimeter or better for the total receiver. A recently modified fiducial mark projection system gives positional accuracy in the image plane to within 10 microns. In object space, this corresponds to a positional accuracy of 1.3 millimeters.

ANALYTIC METHOD

The type of optical data being sought initially was beam intensity as a function of position on a horizontal and a vertical diameter of the parabolic mirror. Various films had been tested to determine the dynamic range and gamma of the linear portion of the characteristic curve of the film. For each type of film and exposure time, a particular absolute intensity variation of the step wedge covers the dynamic range

11

or usable portion of the film curve. One of the brighter steps gives an intensity at the top of the dynamic range of the film. Neutral density filters were inserted at the optical receiver until the most intense radiation corresponds to the intensity of the brightest usable step. After the data were taken and the film developed, the individual frames were scanned consecutively on a densitometer. The scans were always over the same 2 diameters of the parabolic mirror. The densities as a function of position were recorded and then converted to relative intensities through the characteristic curve of the film obtained from the step wedge.

A series of trial photographs were made to determine the feasibility of the technique. The path length is 549 meters, averaging about 2 meters above short grass. The location was the Electromagnetic Propagation Range at the BRL. The range features an extensive array of meteorological sensors with an electronic data acquisition system (Figure 2).

Figure 2. Electromagnetic propagation range with
30-foot sensor stations

Figure A-1 in the Appendix shows a mottled pattern typical for a day with high scintillation. The step wedge extends vertically in the optical system. Since the system incorporates an optical flat, there is a horizontal, but not a vertical, image inversion. Thus, the image can be understood to be the intensity distribution that would be seen if

11

a 2-foot section of ground glass were to be substituted for the parabolic mirror with the observer located behind the ground glass looking back toward the source. This photograph was taken in the summer during a mid-afternoon. The exposure time for all of the photographs is 1/500 second. There was, therefore, no image blur in the horizontal direction. Figure A-2 is a photograph taken at night under medium scintillation conditions. Since the atmosphere was fairly quiet, the high degree of coherence of the laser was maintained, resulting in the characteristic diffraction effects from dust particles on the lenses.

Figure A-3 shows an example of a fleeting optical effect observed after dusk one summer evening. The pattern consisted of large, slowly changing cells which built up gradually, lasting in this condition for about a minute. The pattern broke up quickly into much higher spatial frequencies; once more built up to the large cell structure for a minute; and finally broke up altogether.

Figure A-4 shows one of two photographs of which a quantitative analysis has been made. The step wedge at the left of the photograph was scanned and a computer-fitted characteristic curve derived (Figure A-5). The relative densities are plotted vertically and the logarithm of the exposure is shown to the right. The antilogs are also given. The extremes of the exposure are indicated for the horizontal scan through the mirror. Using this curve, the output of the densitometer was computer-corrected to relative intensities, and plotted (Figure A-6).

THEORY AND RESULTS

Tatarski[1] predicts the two-dimensional spatial spectral densities in a plane perpendicular to the direction of propagation for a plane, monochromatic wave. The spatial spectral densities are postulated to be isotropic and to be a function only of the wavelength, λ, and the path-length, L. For the case where the wind direction angle relative to the optical path is much larger than the quantity $(\lambda/L)^{1/2}$, the intensity structure is assumed to be "frozen-in" and carried across the optical

13

path by the normal wind component, v_n. Tatarski thus translates from a two-dimensional spatial, spectral density domain to a one-dimensional time domain.

In Tatarski's experiment, a weakly divergent incandescent beam is propagated over a homogeneous path within 2 meters of the ground. The received light is monitored by a photocell with an aperture small enough (2 millimeters) to resolve the highest spatial frequencies. As the normal wind component takes the turbulent medium across the beam path, a one-dimensional intensity profile is recorded. Since the optical path is near the ground, the vertical wind component is necessarily small, so that the profile is predominantly horizontal. The magnitude of v_n is monitored during the experiment. Figure A-7 shows the results of such measurement. The output of the photocell is sent into a time spectrum analyzer. The power, $W(f)$, is multiplied by temporal frequency and plotted versus the $\log_2$ of the temporal frequency. As can be expected, as v_n goes to higher values, the peak power point of the curve also moves to higher frequencies. Next, all these curves, along with data taken at different pathlengths, are normalized to a v_n of 1 meter per second and a path of 1,000 meters (Figure A-8). The curves then assume, generally, the same shape.

Tatarski's time spectrum is related to the space spectrum by

$$T = S \cdot v_n \tag{1}$$

where the space spectrum, S, is measured in cycles per meter. When the space spectrum is thus measured, it is equivalent to the time spectrum inherently normalized to a v_n of 1 meter per second. To test this relationship, a power-density, spectrum analysis was made using the horizontal intensity profile shown in Figure A-6. Figure A-9, then, shows the relative powers as a function of spatial frequencies. Next, the power was multiplied by frequency and plotted on a logarithmic abscissa (Figure A-10). Since the spectra have frequency plotted in cycles per meter and are thus normalized for a normal wind component of 1 meter per

14

second, the space spectra units convert directly to time spectra units. The roughness of the curve is indicative of the shortness of the sample length. To get a more definitive plot, many such samples should be analyzed and averaged. In order to approximate the effect of a longer sample length, a smoothing program was applied to Figure A-10 resulting in the curve shown in Figure A-11. This reveals a much greater likeness to the Tatarski time plots but the spatial spectra were normalized by different schemes and the ordinates cannot be compared. With this method of data acquisition there is no time lag from the beginning of the intensity scan to the end so no assumption about the degree to which the turbulent cell structure is "frozen-in" is necessary to infer the nature of the true spatial frequency characteristics. Under the assumption that the photograph was indeed isotropic, the unsmoothed vertical and hori- zontal power density spectra were averaged, multiplied by frequency, and plotted on a logarithmic abscissa (Figure A-12). These combined spectra units were then smoothed (Figure A-13), and it was this curve that was used for comparison to the theory.

By the same process, a photograph taken during a night propagation run was also analyzed (Figure A-14). As in the earlier photograph taken at night, Figure A-2, the effect of highly coherent light operating on the optical receiver can be seen as diffraction rings in the image plane. Figure A-15 shows the power density spectrum, and Figures A-16 to A-19 show the frequency plots smoothed and averaged as before.

Tatarski predicts that the frequency at which the maximum power occurs is given by the formula

$$f_m = A \frac{v_n}{(\lambda L)^{1/2}} \tag{2}$$

where f_m is defined as the average of the two frequencies occurring at one-half the peak power. Theoretically, A is given as 0.55, while experimentally Tatarski obtains a value of 0.32. Using Figures A-13 and A-19, an average A of 0.222 was obtained for the two photographs.

Although not explicitly stated later in Tatarski, f_m is derived for a plane wave source. The difference between the theoretical and experimental values is not explained. If, in a very simple model, all of the diffraction is assumed to take place at a plane located midway between the transmitter and receiver, then the spatial frequencies will be scaled down at the receiver by the ratio of the beam width at the path midpoint to the beam width at the path terminus. As transmitted light is changed from a collimated beam to a point source, B goes from a value of 1.0 to 5.0. Table I shows this "divergence factor" for both experiments. This then is to be applied as a correction factor to the coefficient 0.55 for a plane wave. The product of these two is in the column titled "A, calculated." This value can be compared with the measured value of A.

Table I

$$A = B(0.55) \qquad B = \frac{\text{width of beam at midpoint}}{\text{width of beam at terminus}} = \text{divergence factor}$$

	$B_{\text{calculated}}$	$A_{\text{calculated}}$	A_{measured}
Plane Wave	1.0	0.55	--
Tatarski	0.6	0.33	0.32
BRL	0.504	0.277	0.222

The importance of resolving the highest spatial frequencies in object space was inferred earlier. The influence of the diameter of the photocell aperture on the frequency distribution has been predicted by Tatarski and measured by others.[2] With the present demagnification from object space to the image plane and the size of the scanning aperture of the densitometer, the effective aperture size in object space is 1.26 millimeters. To show the effect of an increasing one-dimensional aperture, the intensities shown in Figure A-6 were averaged over windows with widths of 5, 9, 17, and 33 samples. Each of the smoothed scans was subjected to frequency analysis, smoothed, and plotted (Figure A-20). The smoothed frequency times power plot of Figure A-11 is also shown for

16

comparison. The effective sizes of the apertures in increasing widths are 1.26, 5.16, 9.07, 16.9, and 32.5 millimeters. As the widths are increased, both the decrease and shift in peak power and the loss of high frequency response are readily apparent.

The shape and maxima of the spatial frequency spectra are not supposed to vary for a given pathlength or wavelength. However, the intensities, which are postulated to be log normally distributed, are predicted to exhibit a variance proportional to the fluctuations in the index field. Tatarski's formula giving this relationship is

$$\sigma^2 = 1.23 \ C_n^{\ 2} \ k^{7/6} \ L^{11/6} \tag{3}$$

where σ is the standard deviation of the log normal distribution, C_n is the index structure constant, k is the wave number of the light, and L is the pathlength. To test this relationship, the horizontal intensities from Figures A-4 and A-14 were each normalized by division of their average intensity. The percent number of occurrences was then plotted versus the normalized intensities to form distribution curves (Figures A-21 and A-22). Figure A-21 from the afternoon propagation data shows a much greater skewness, indicating higher scintillation conditions. Next, the integral of each of these curves was taken to yield the cumulative distribution curves. The integrated percent occurrences were plotted on probability paper versus the log of the normalized intensities (Figures A-23 and A-24). Both sets of data conform closely to log normal distributions. The divergence at the extremes of the curve in Figure A-23 can be interpreted in the following way. The first point was taken from the very edge of the mirror where the calibration has indicated a sharp attenuation of intensities due to vignetting. The intensities at the upper end of the curve came from the top of the characteristic curve. Since they were forcing the dynamic range of the film, their true values were likely higher than those indicated. Although no C_n was measured for the two cases, the cumulative distribution curves were used to derive the standard deviation. Equation (3) was solved for C_n, and the appropriate values were inserted; Table II lists the results.

17

Table II

	σ	C_n (calculated)
Afternoon	0.852	$1.96 \times 10^{-7} \ m^{-1/3}$
Night	0.332	$7.63 \times 10^{-8} \ m^{-1/3}$
[3]Weak turbulence		$C_n = 8 \times 10^{-9} \ m^{-1/3}$
Intermediate turbulence		$C_n = 4 \times 10^{-8} \ m^{-1/3}$
Strong turbulence		$C_n = 5 \times 10^{-7} \ m^{-1/3}$

Comparing the calculated values of C_n with those given by Davis[3] for
three representative cases indicates reasonable agreement for the inter-
mediate to strong scintillation conditions.

SUMMARY AND CONCLUSION

Initial data analysis of the spatial intensity distributions from
the optical receiver shows a high degree of correlation to the theoreti-
cal predictions of Tatarski. When the divergence of the transmitted beam
is taken into consideration, the predicted frequency of maximum power
compares favorably with the measured value. Widening of the sampling
aperture is shown both to attenuate the high frequency resolution and to
shift the peak power point to lower frequencies. Calculated values of
the index-structure constant from the measured variance of the intensity
profiles conform to the proper orders of scintillation magnitude.

During normal data runs, a time series of photographs is taken to
make the results statistically meaningful. Since in this particular
approach the scanning is not a function of the normal wind component,
any intensity profile can be examined, including the vertical, allowing
a check of the assumption of optical isotropy both by electronic reduction
and direct optical correlation techniques. By this method, the spatial
frequency domain may be converted to a temporal frequency domain which
is inherently normalized for a wind component normal to the direction of

beam propagation of 1 meter per second. No assumption about the degree
to which the turbulent cell structure is "frozen-in" is necessary to
infer the nature of the spatial frequency statistics. In addition, the
high resolution and good signal-to-noise characteristics of the receiver
make accurate measurements of beam pointing reliability possible for
various system applications.

This BRL approach will help to give a better quantitative under-
standing of the constraints placed on nearly all optical systems working
in the atmosphere.

REFERENCES

1. V. I. Tataraki, "Wave Propagation in a Turbulent Medium,"
   McGraw-Hill, 1961.

2. See D. J. Portman, F. C. Elder, E. Ryznar and V. E. Noble, "Journal
   of Geophysical Research," Vol. 67,3290, 1962.

3. J. Davis, "Applied Optics," Vol. 5, No. 1, January 1966, p 141.

20

- APPENDIX

FIGURES
(Atmospheric Effects on Laser Beams)
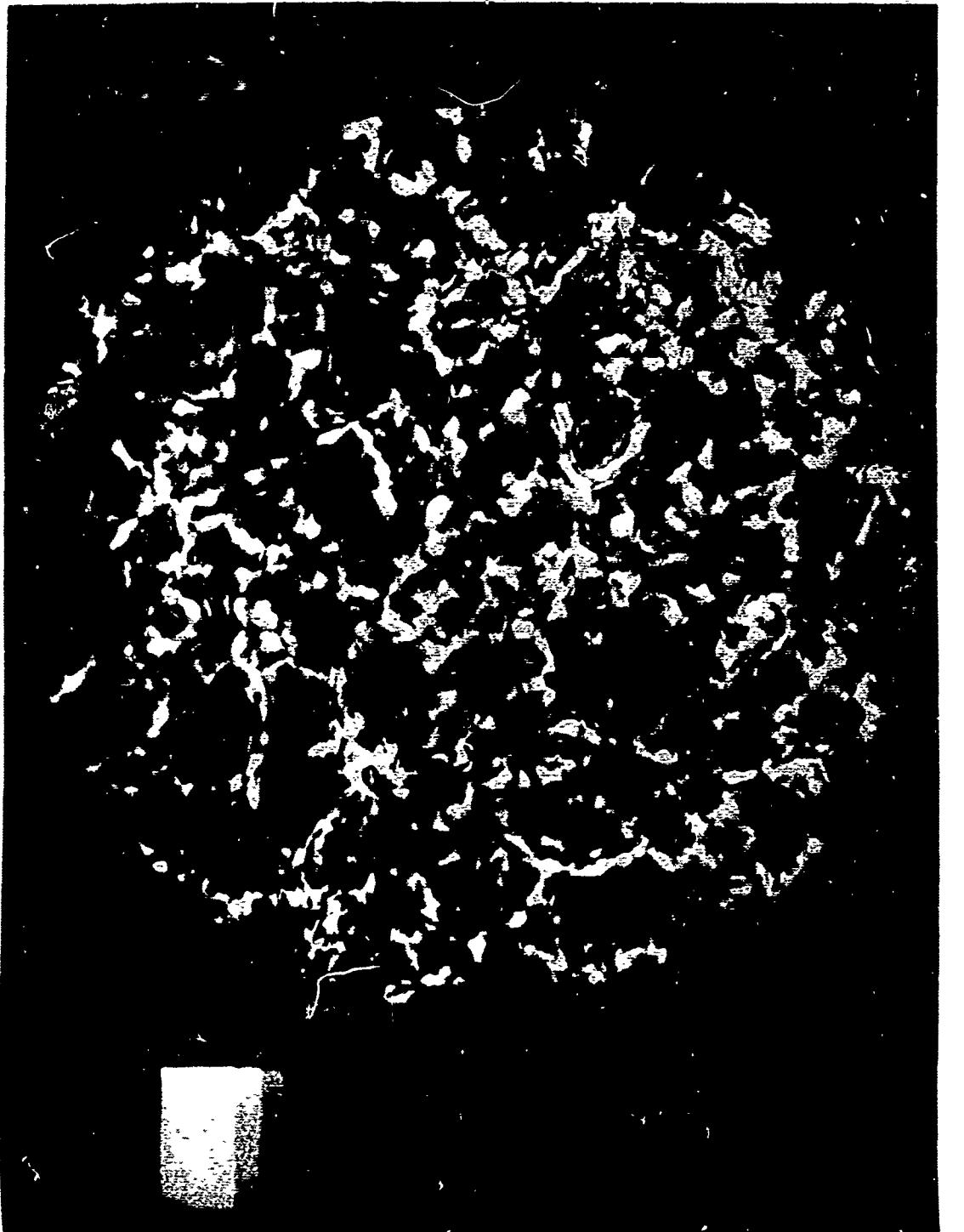
Figure A-1. Beam cross-section photograph taken under high
scintillation conditions
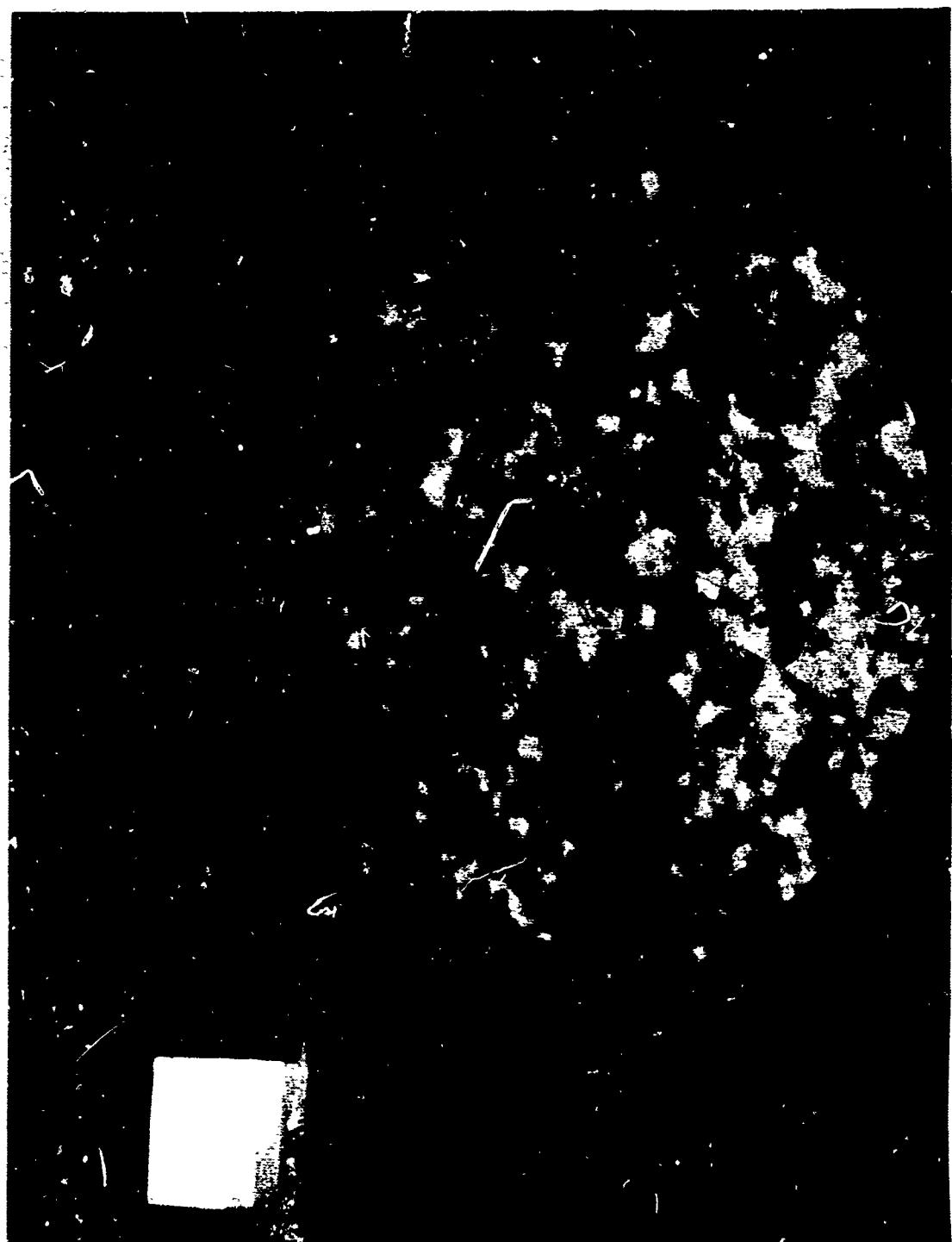
Figure A-2. Beam cross-section photograph taken under medium
scintillation conditions

24
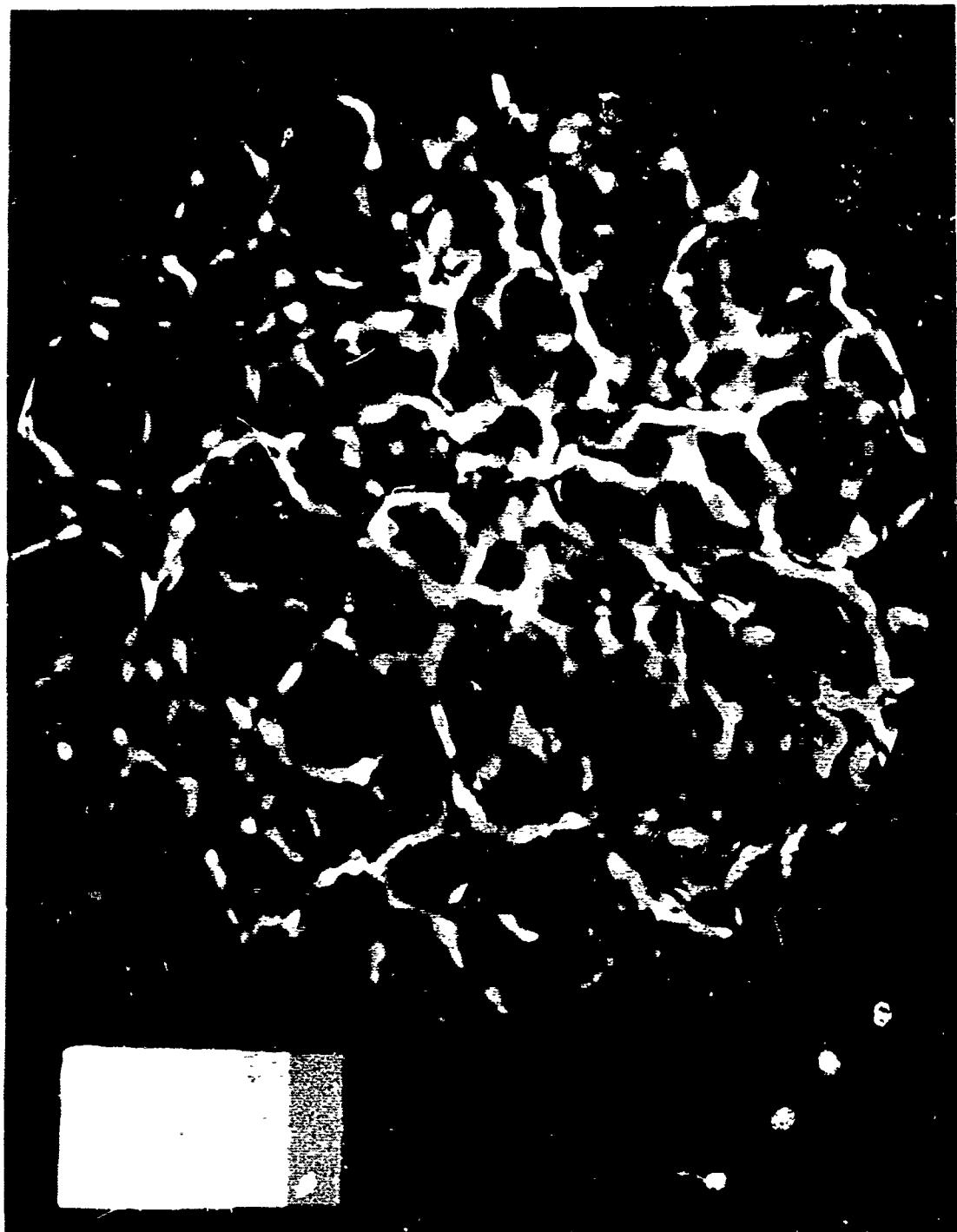
Figure A-3. Beam cross-section showing unusually large cell structure
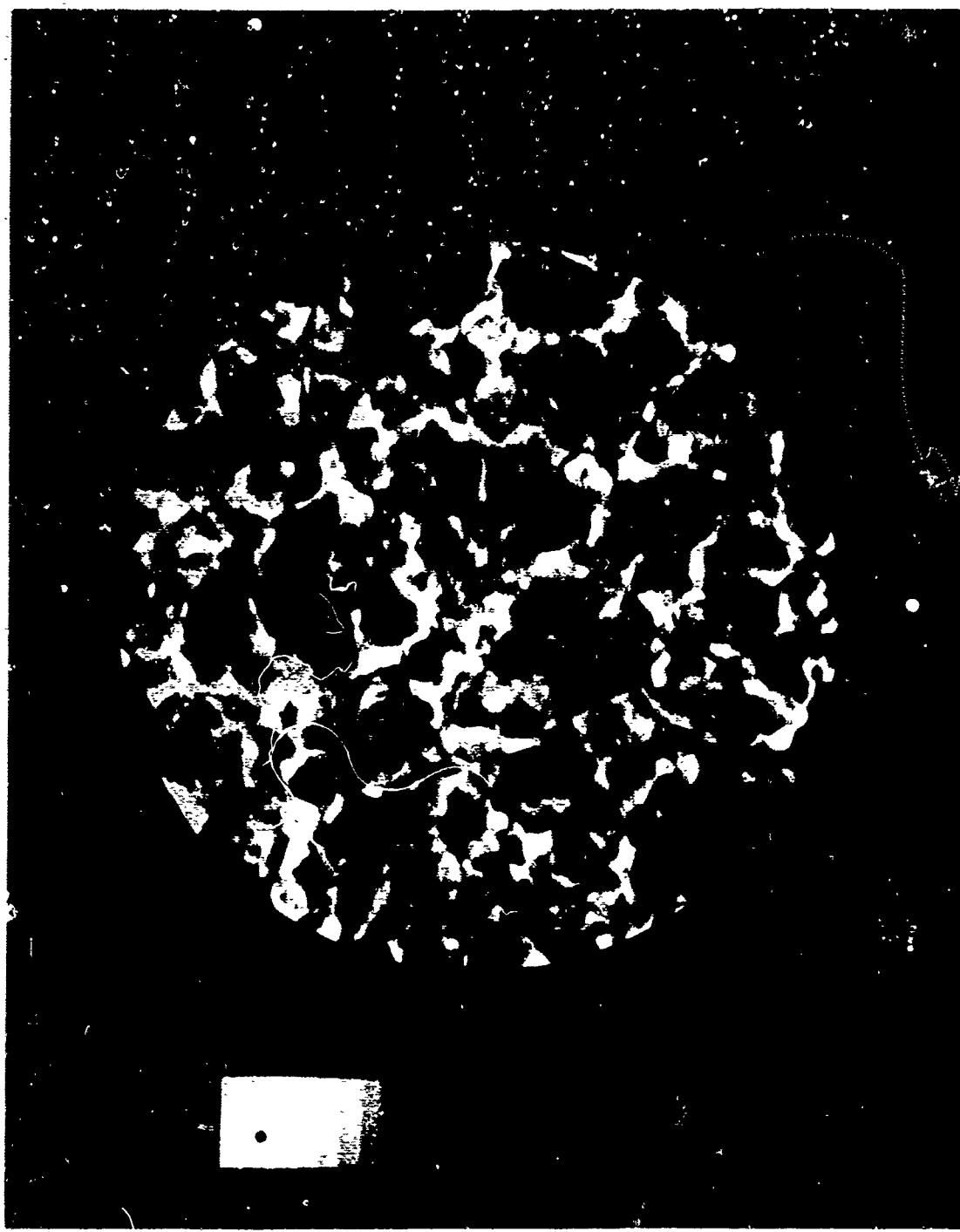
Figure A-4. Sample of beam cross-section data used for quantitative
analysis (afternoon propagation)
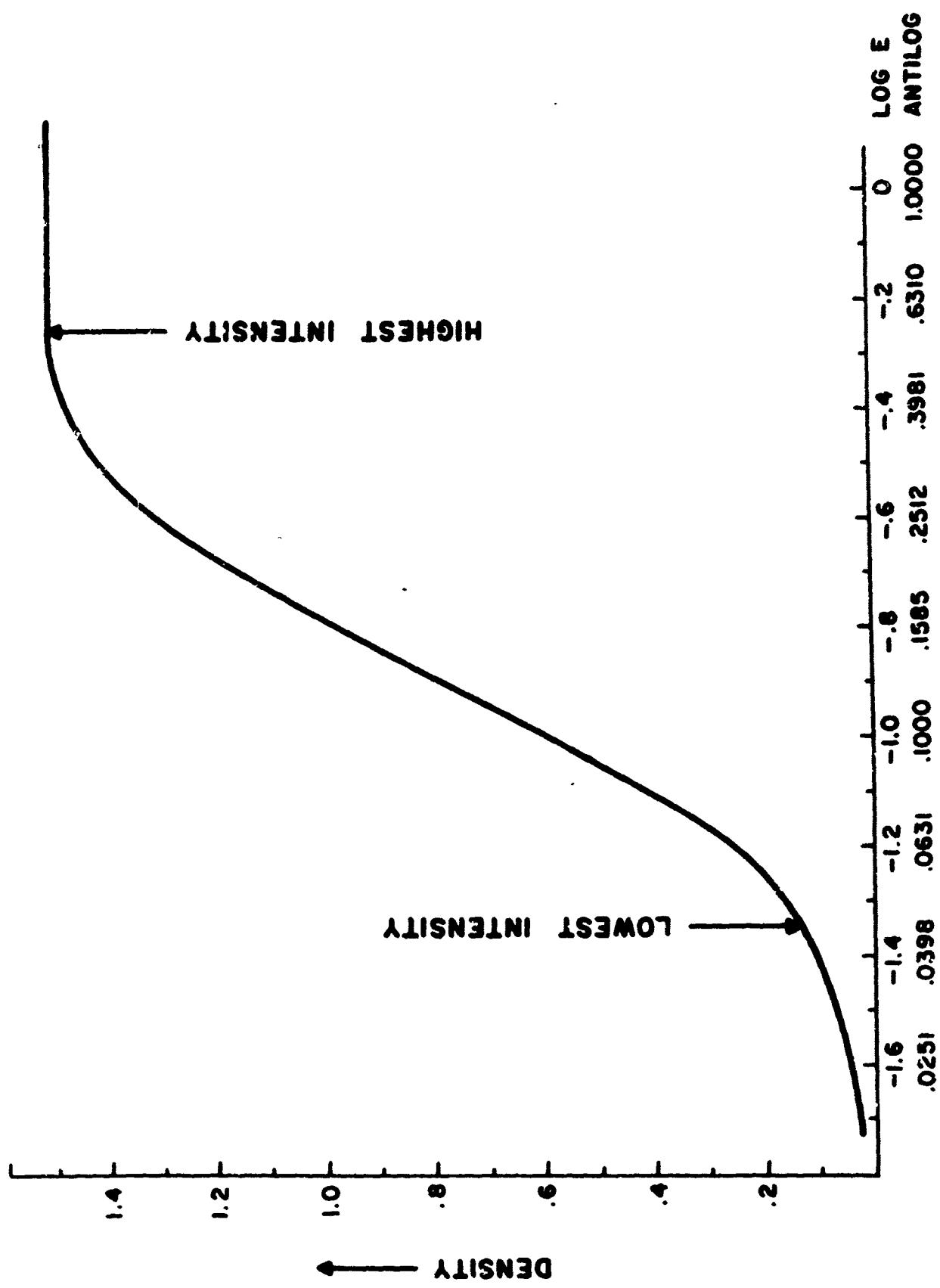
Figure A-5. A computer-derived characteristic curve
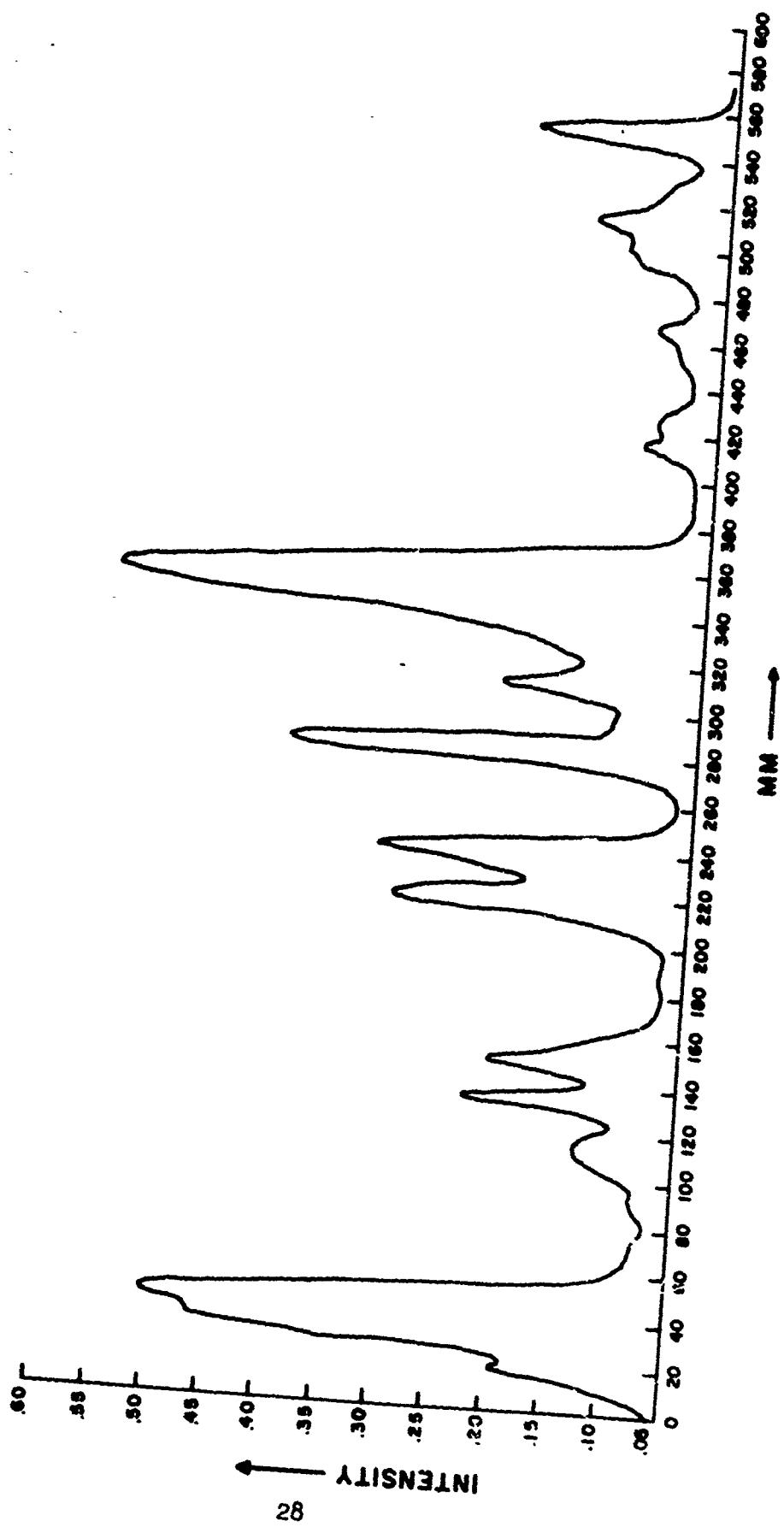
Figure A-6. Horizontal intensity profile of beam cross-section

28
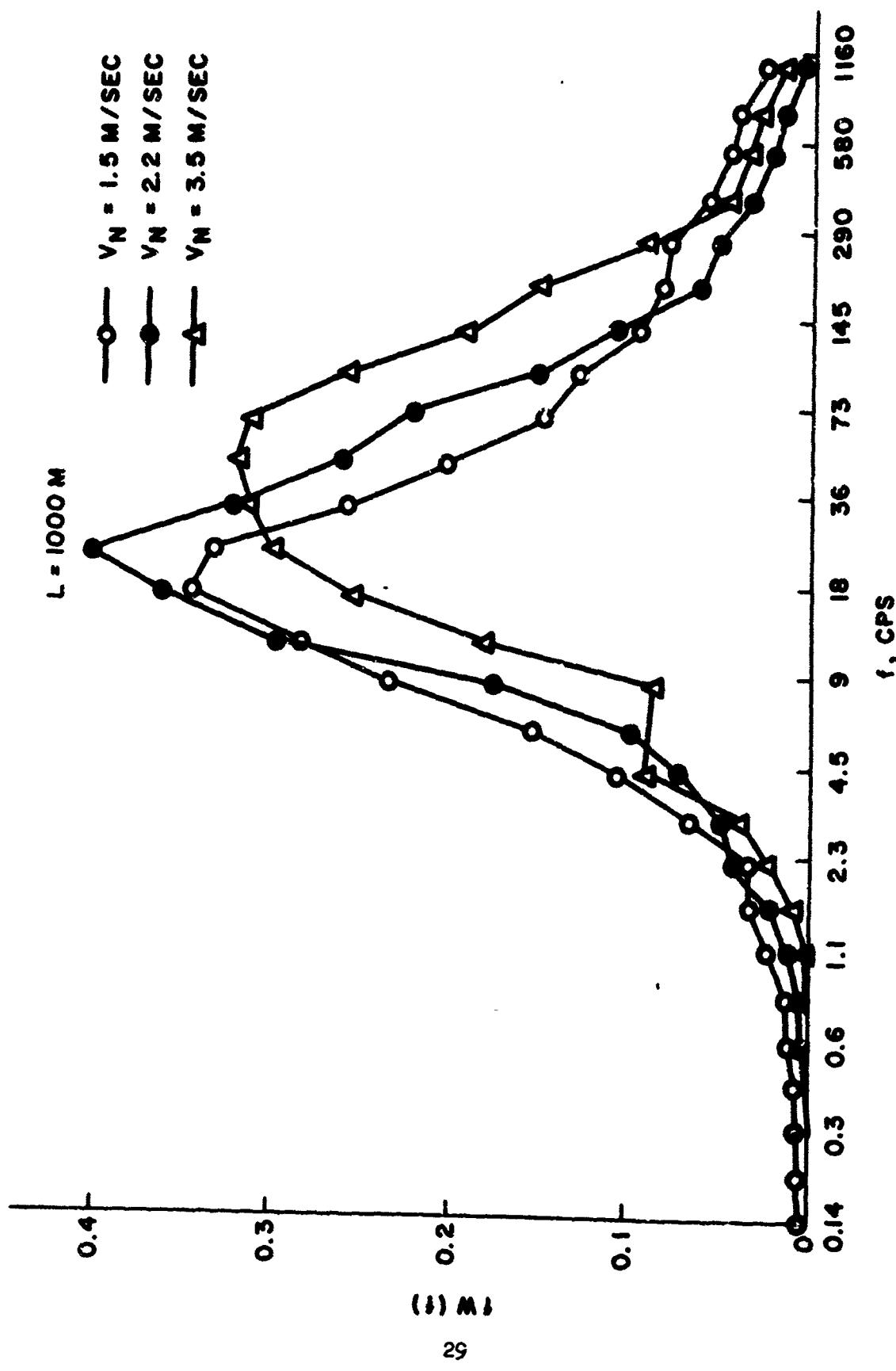
Figure A-7. Temporal frequency times spectral density vs temporal frequency (Tatarski, Wave Propagation in a Turbulent Medium, McGraw-Hill, 1961, page 220)
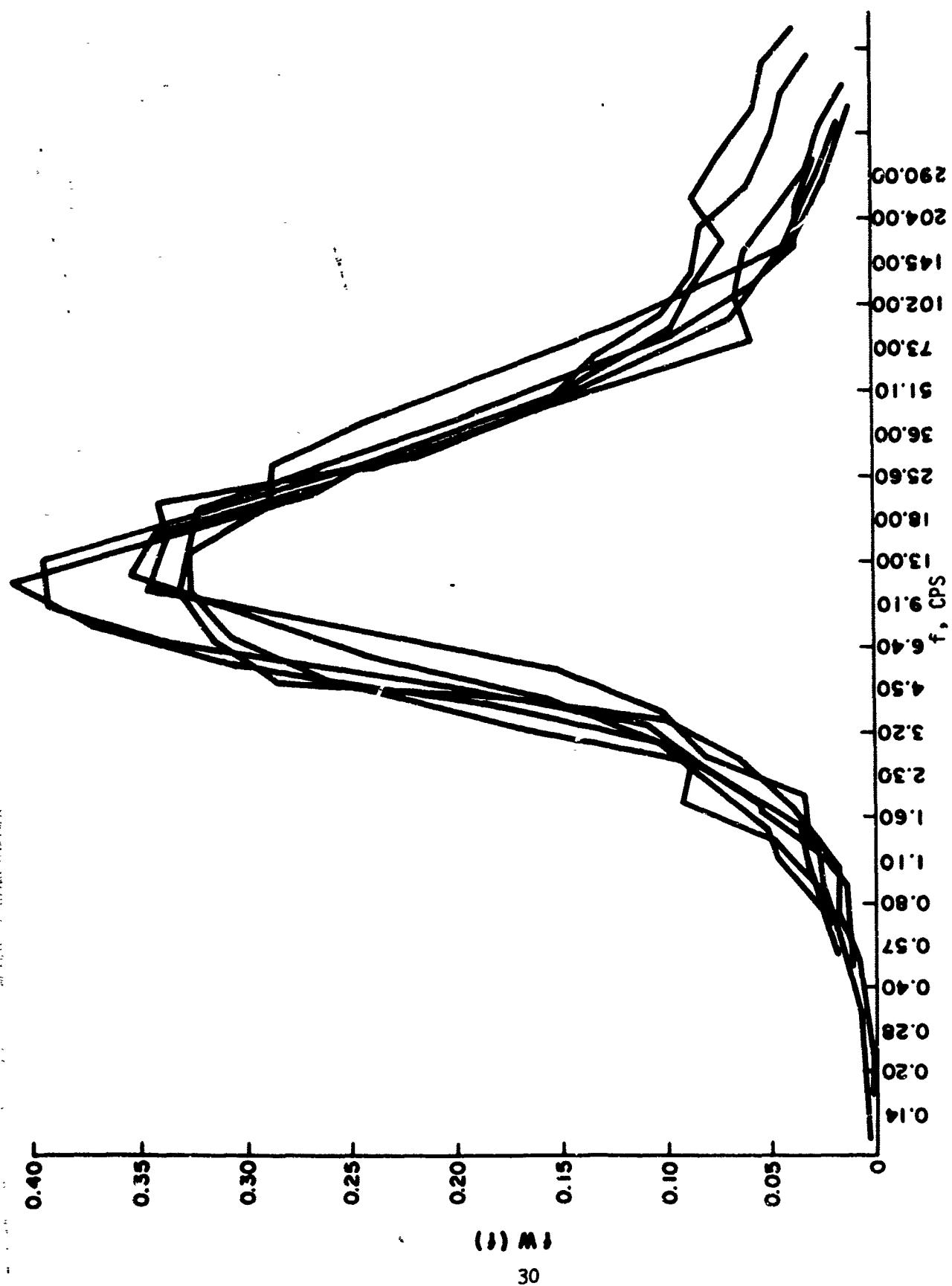
Figure A-8. Temporal frequency times spectral density vs temporal frequency normalized to a normal wind component of 1 meter/second

(Tartarski, Wave Propagation in a Turbulent Medium, McGraw-Hill, 1961, page 222)
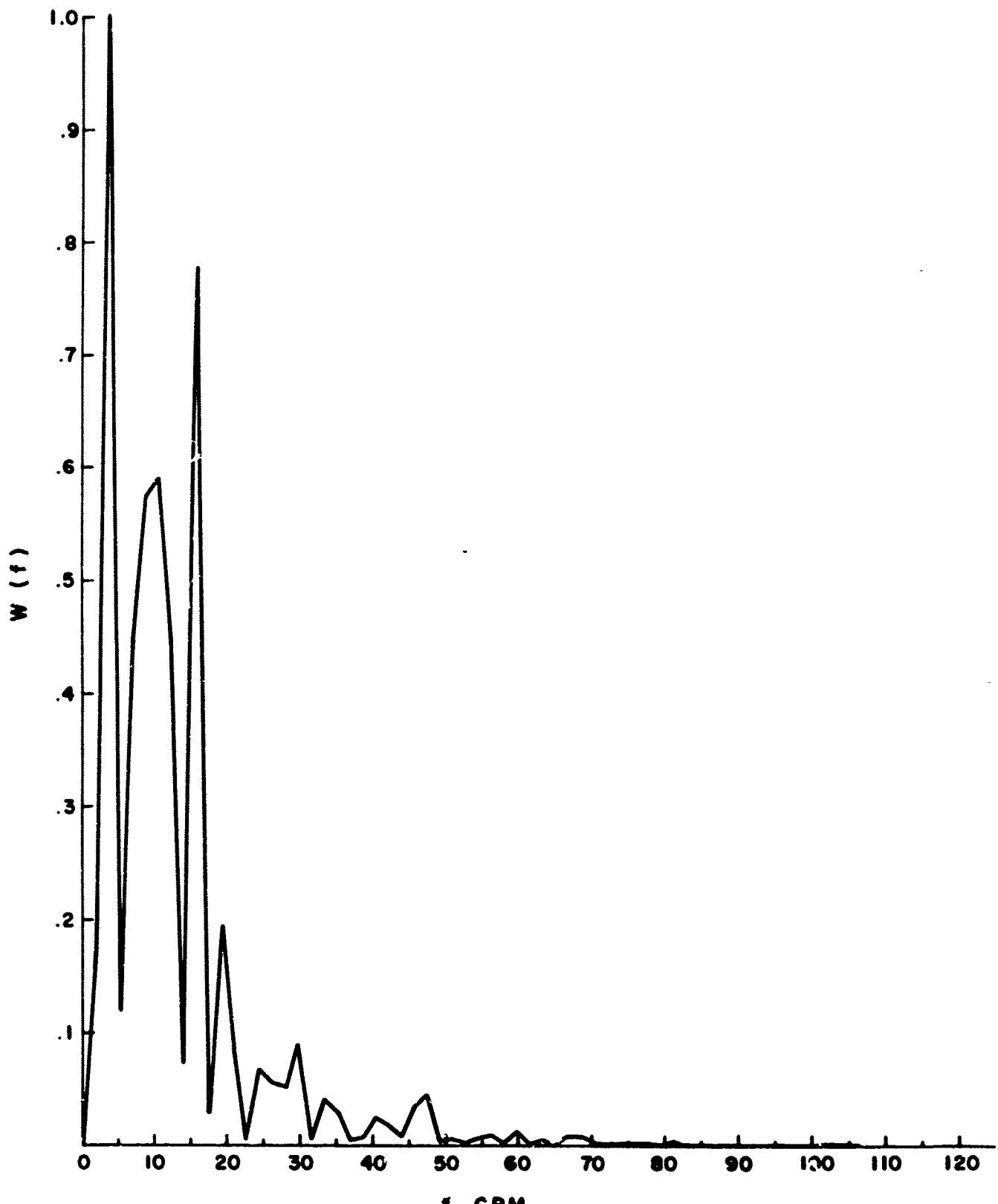
Figure A-9.   Fourier power spectral density plot of horizontal intensity
profile (afternoon propagation)
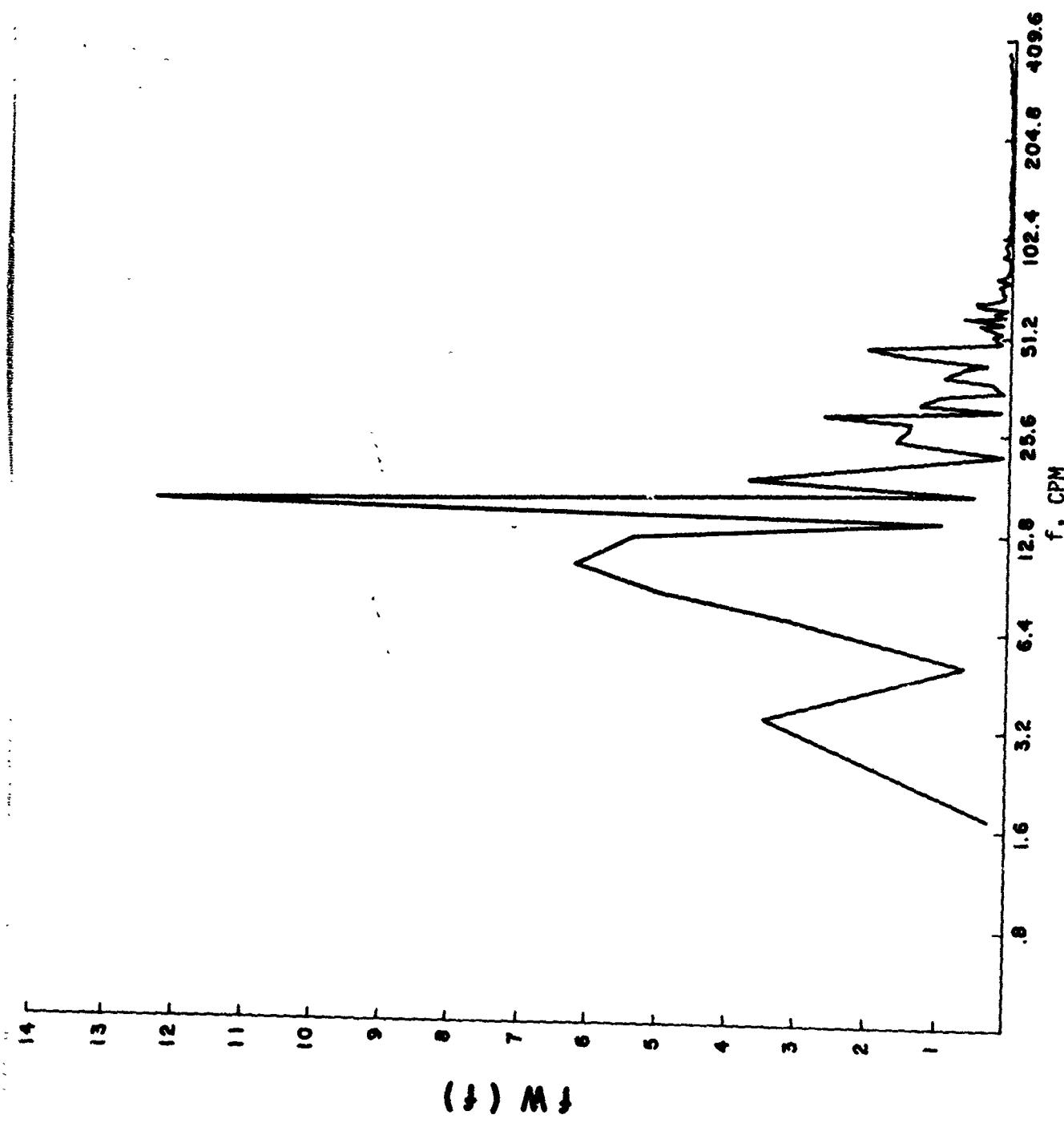
Figure A-10. Spatial frequency times power density spectrum vs spatial frequency (afternoon propagation)
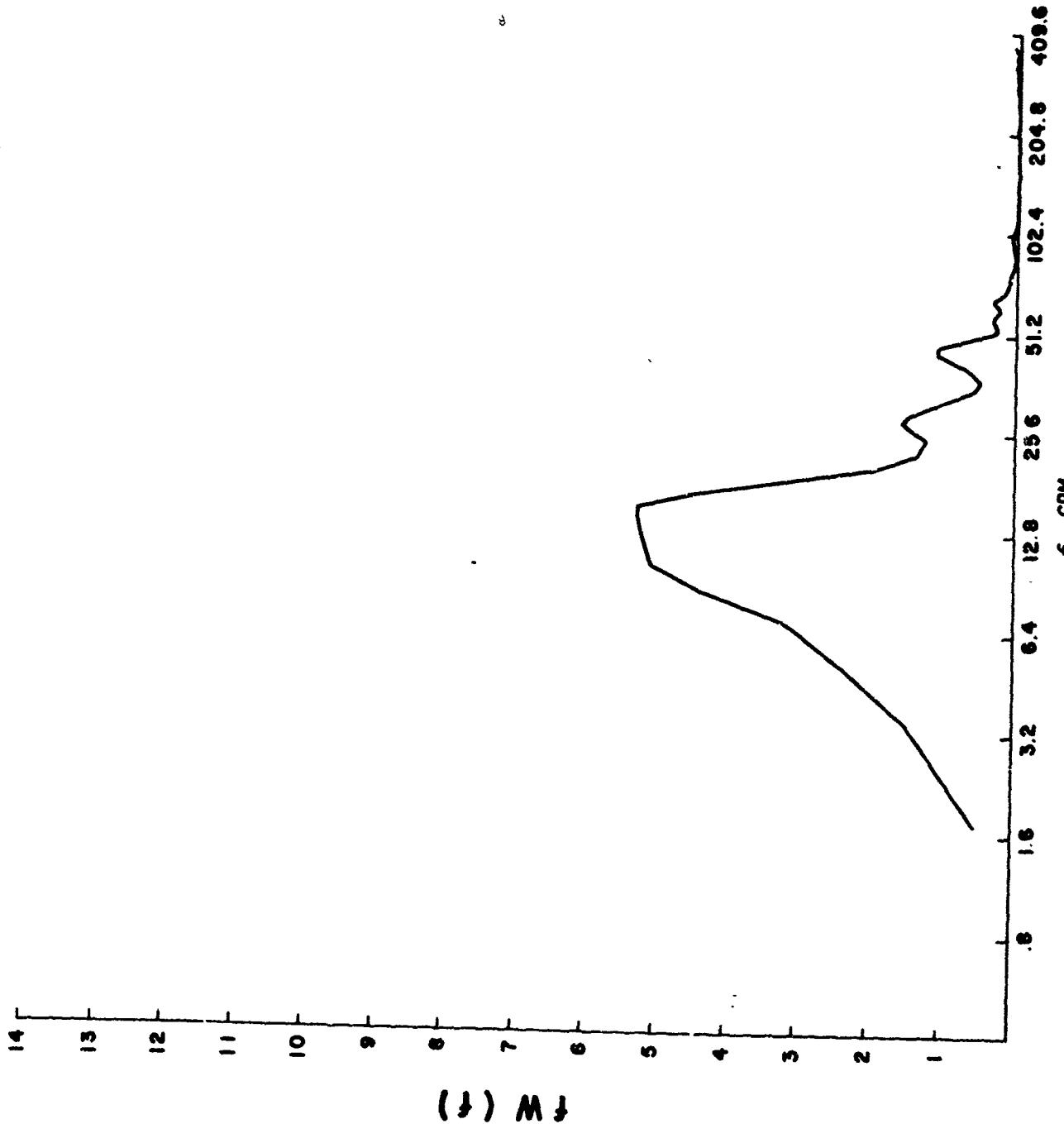
Figure A-11. Spatial frequency times smoothed power density spectrum vs spatial frequency (afternoon propagation)

33
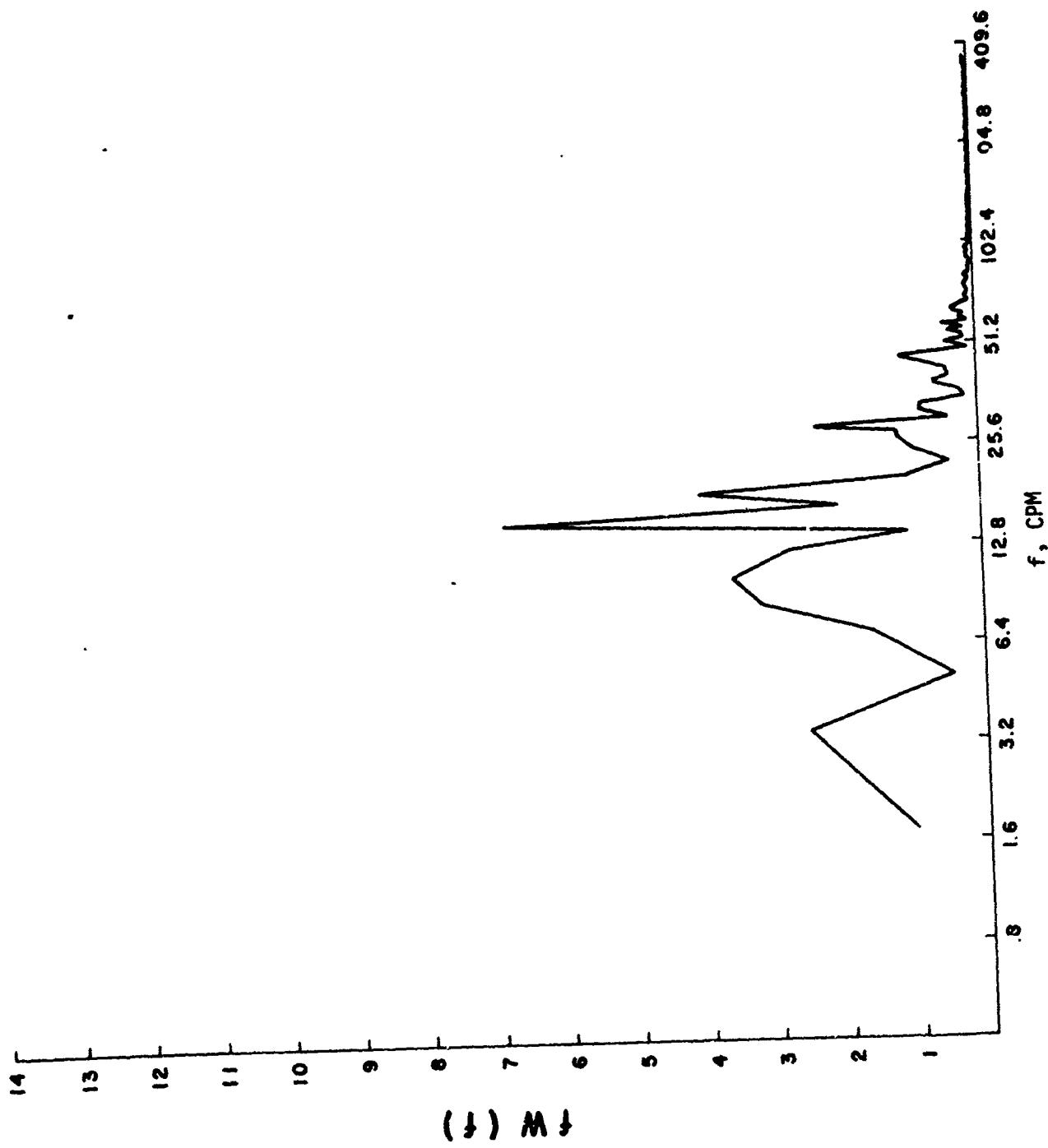
Figure A-12. Spatial frequency times averaged horizontal and vertical power density spectra vs spatial frequency (afternoon propagation).

34
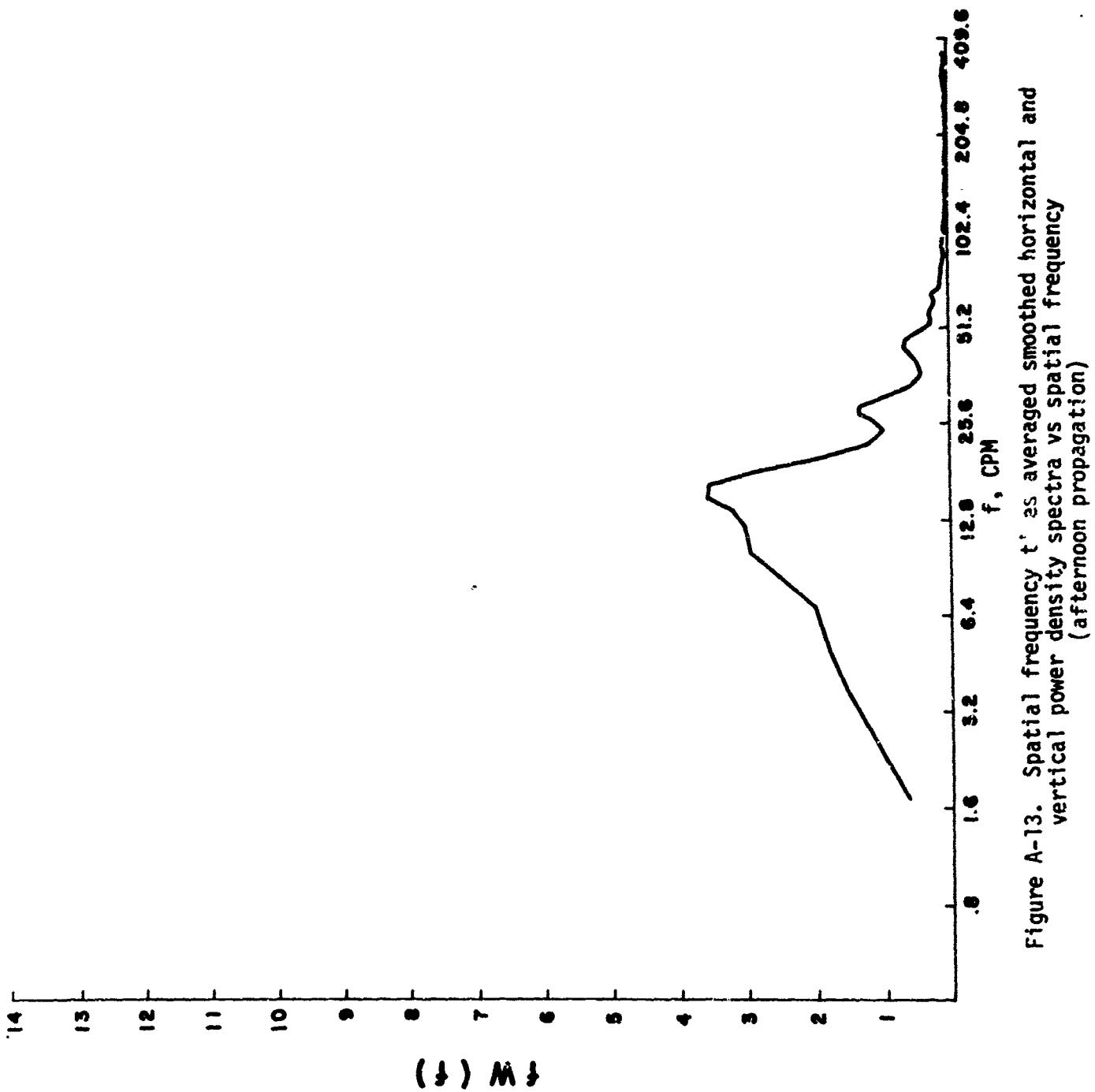
Figure A-13. Spatial frequency t' as averaged smoothed horizontal and vertical power density spectra vs spatial frequency (afternoon propagation)

35
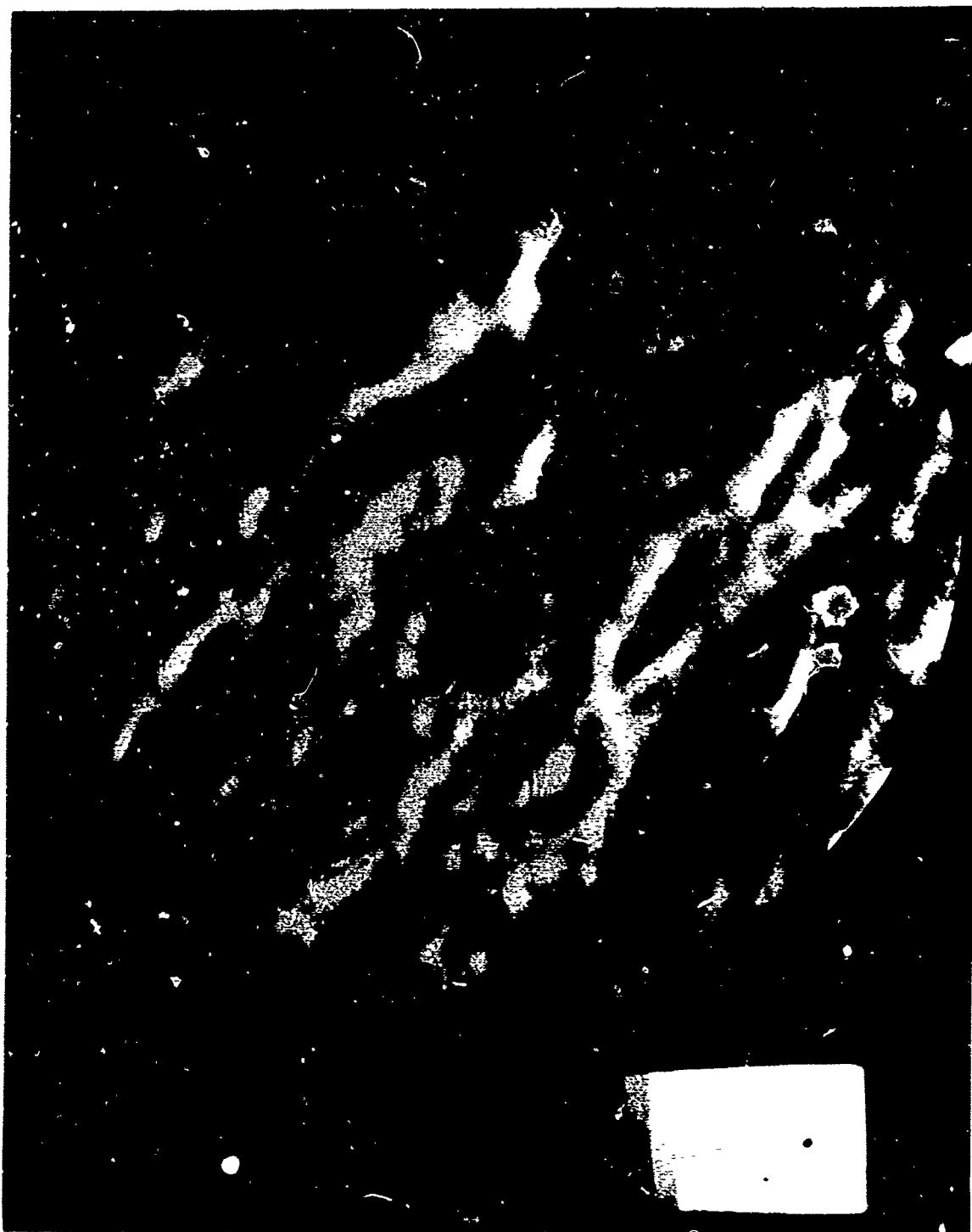
Figure A-14. Sample of beam cross-section data used for quantitative analysis (night propagation)
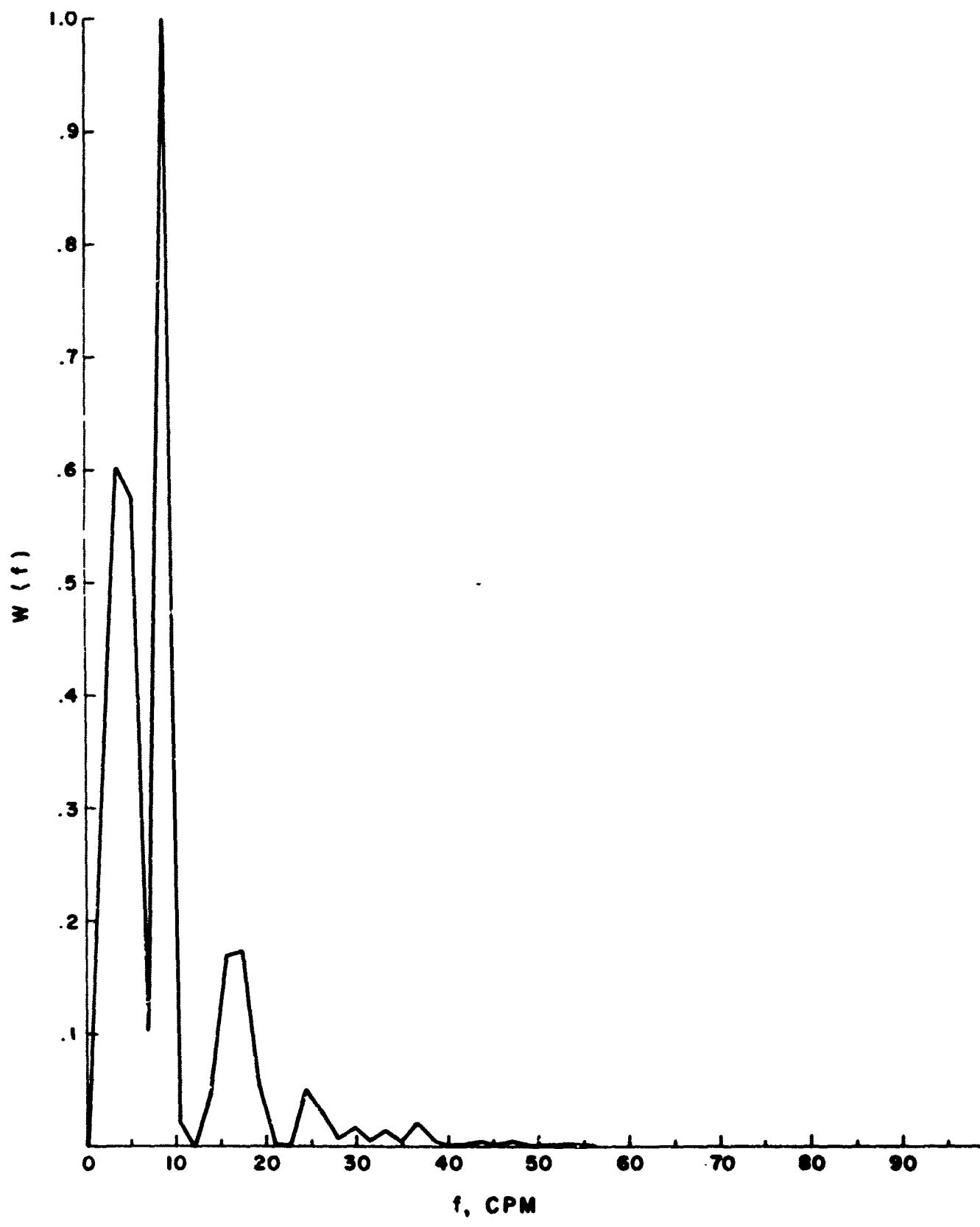
Figure A-15. Fourier power spectral density plot of horizontal intensity
profile (night propagation)

37
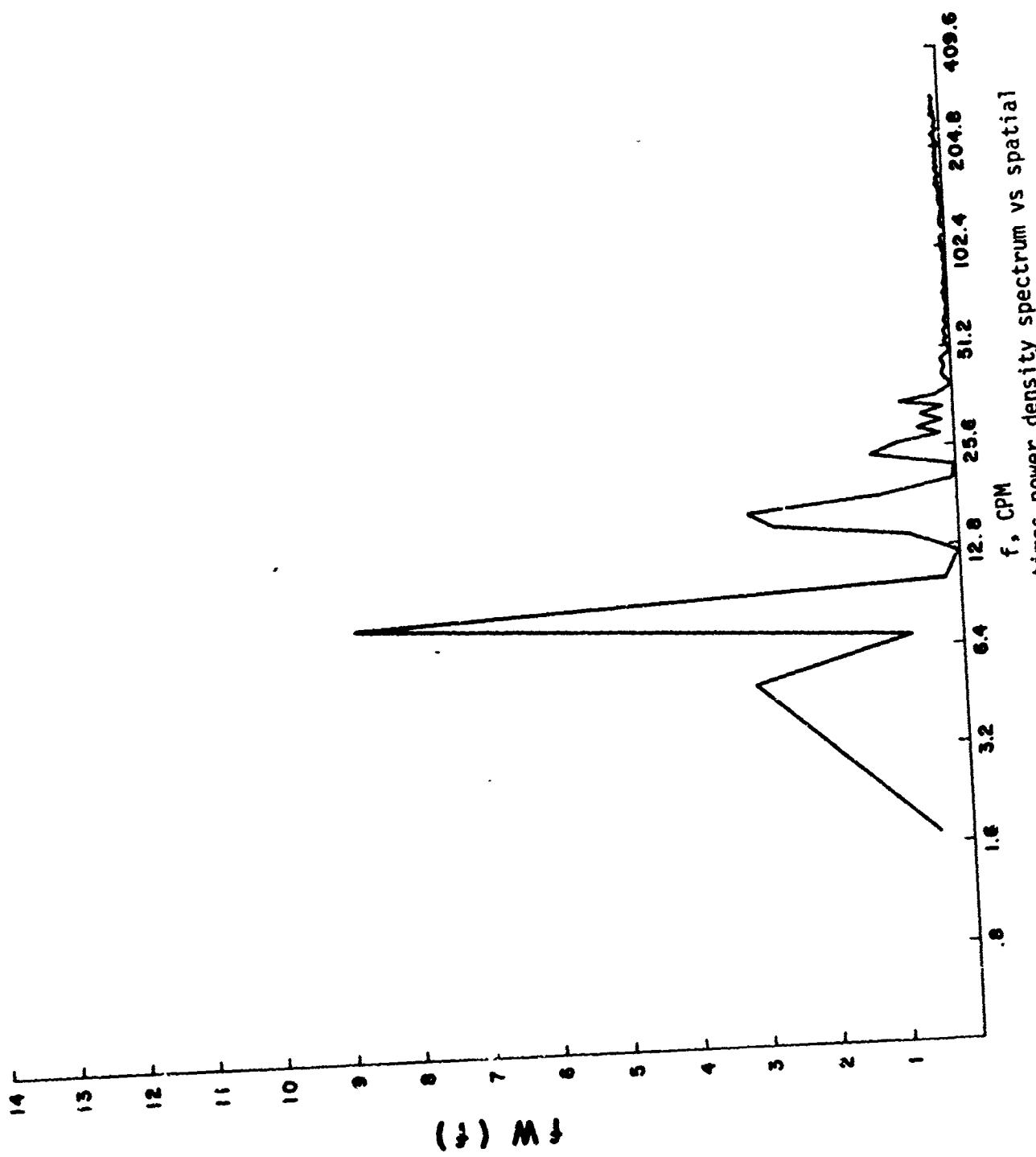
Figure A-16. Spatial frequency times power density spectrum vs spatial
frequency (night propagation)
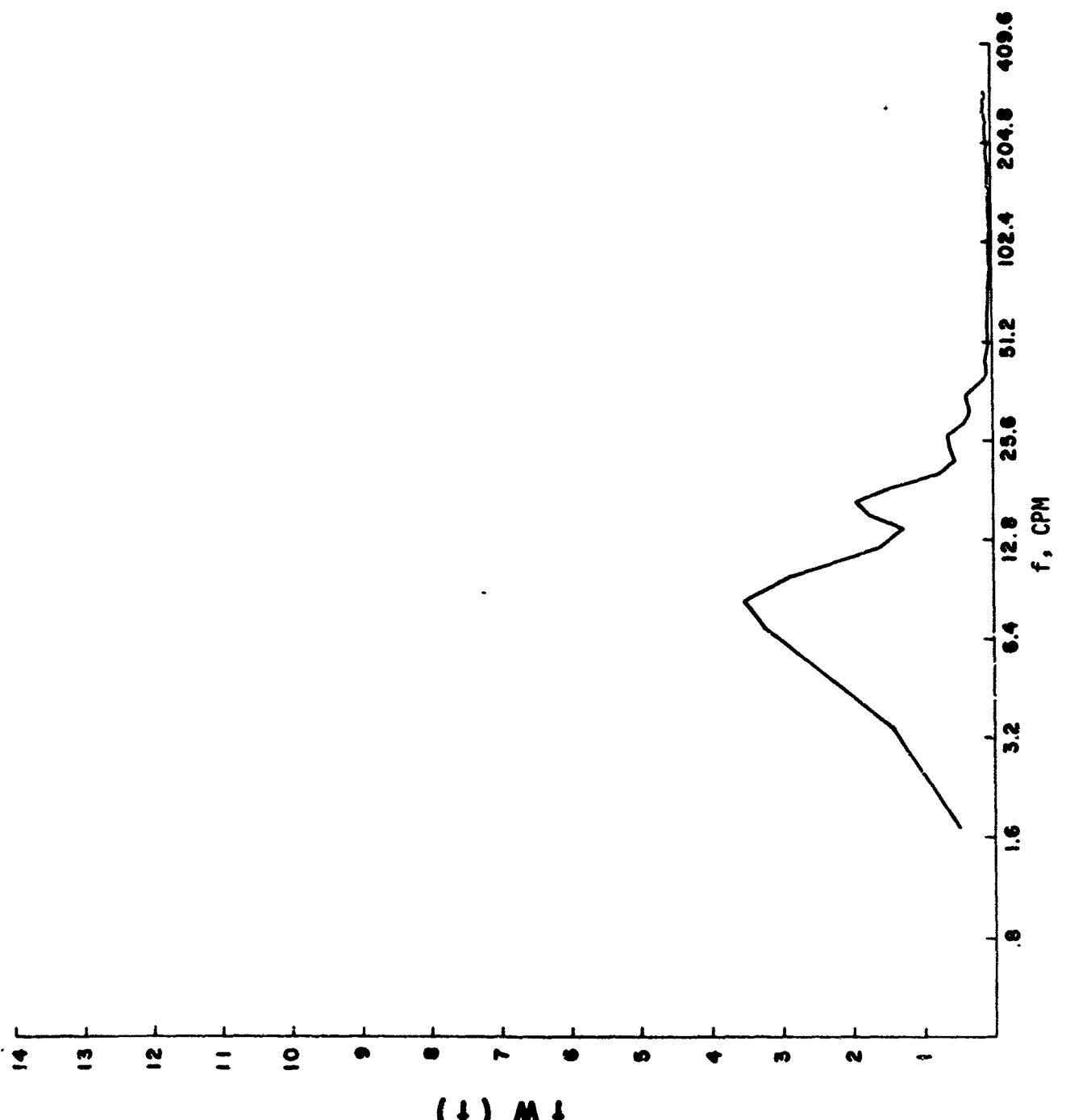
Figure A-17. Spatial frequency times smoothed power density spectrum vs spatial frequency (night propagation)
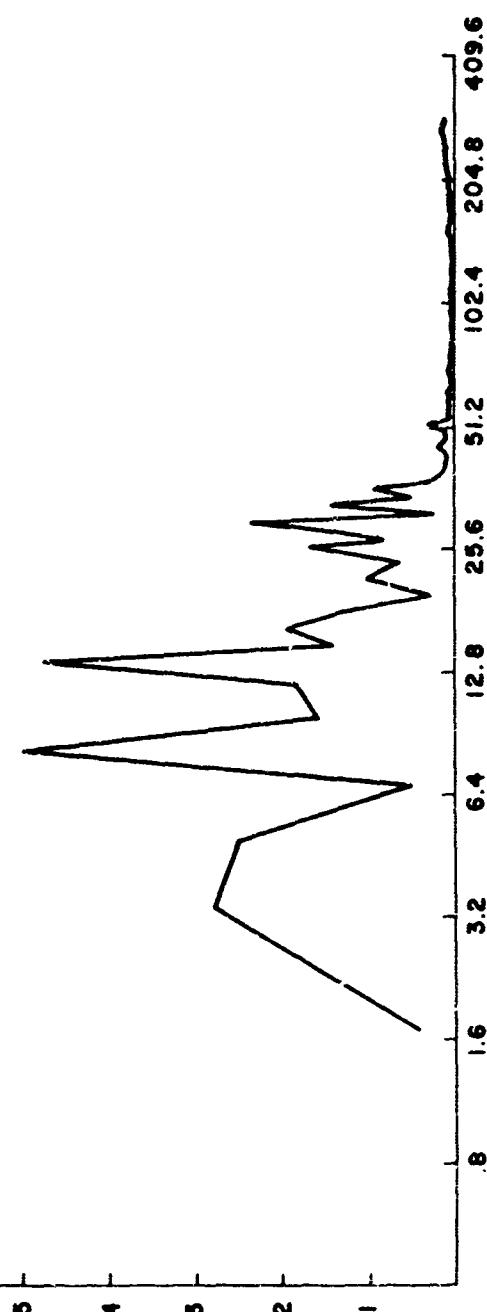
Figure A-18. Spatial frequency times averaged horizontal and vertical power density spectra vs spatial frequency (night propagation)
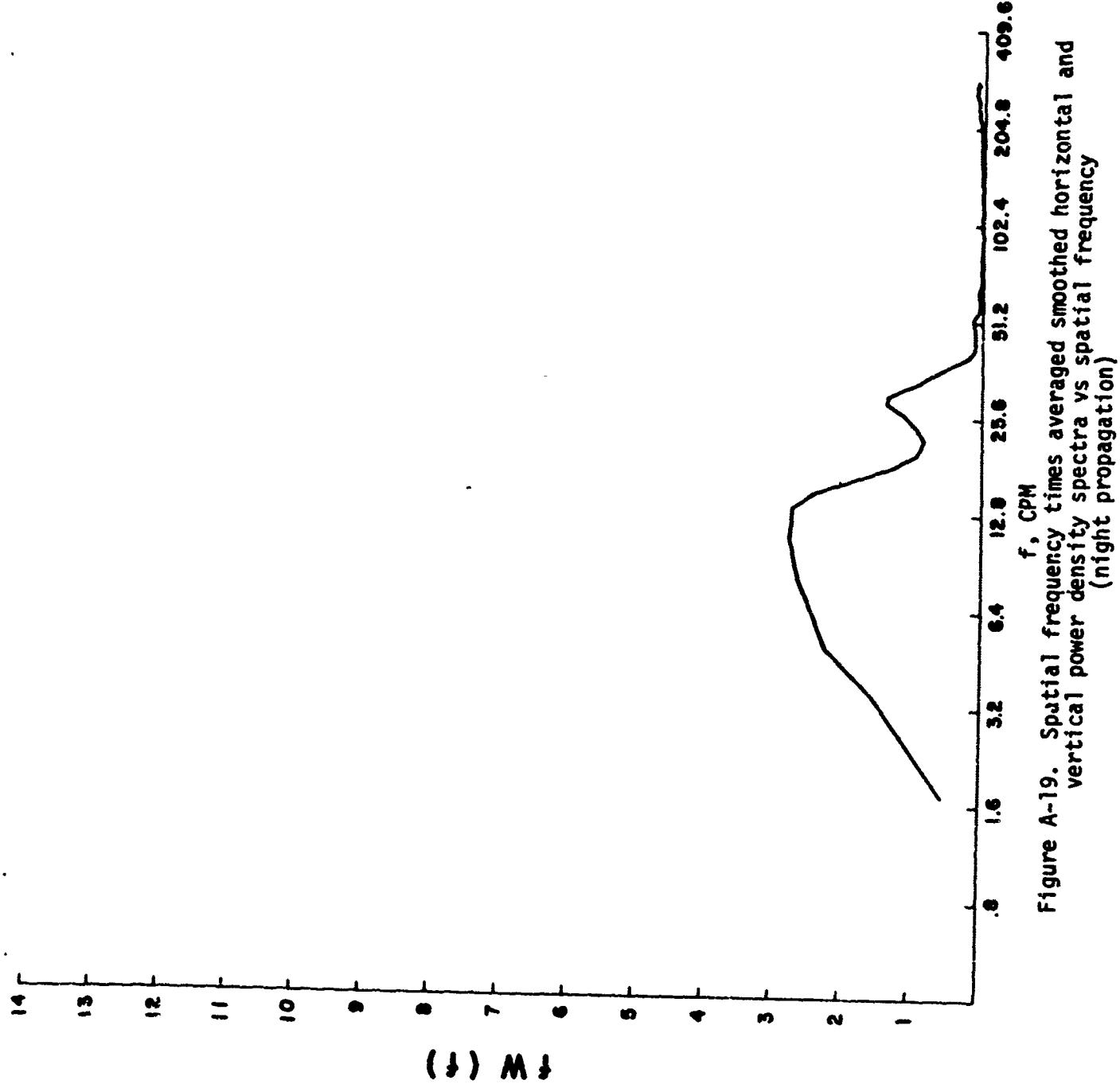
Figure A-19. Spatial frequency times averaged smoothed horizontal and
vertical power density spectra vs spatial frequency
(night propagation)
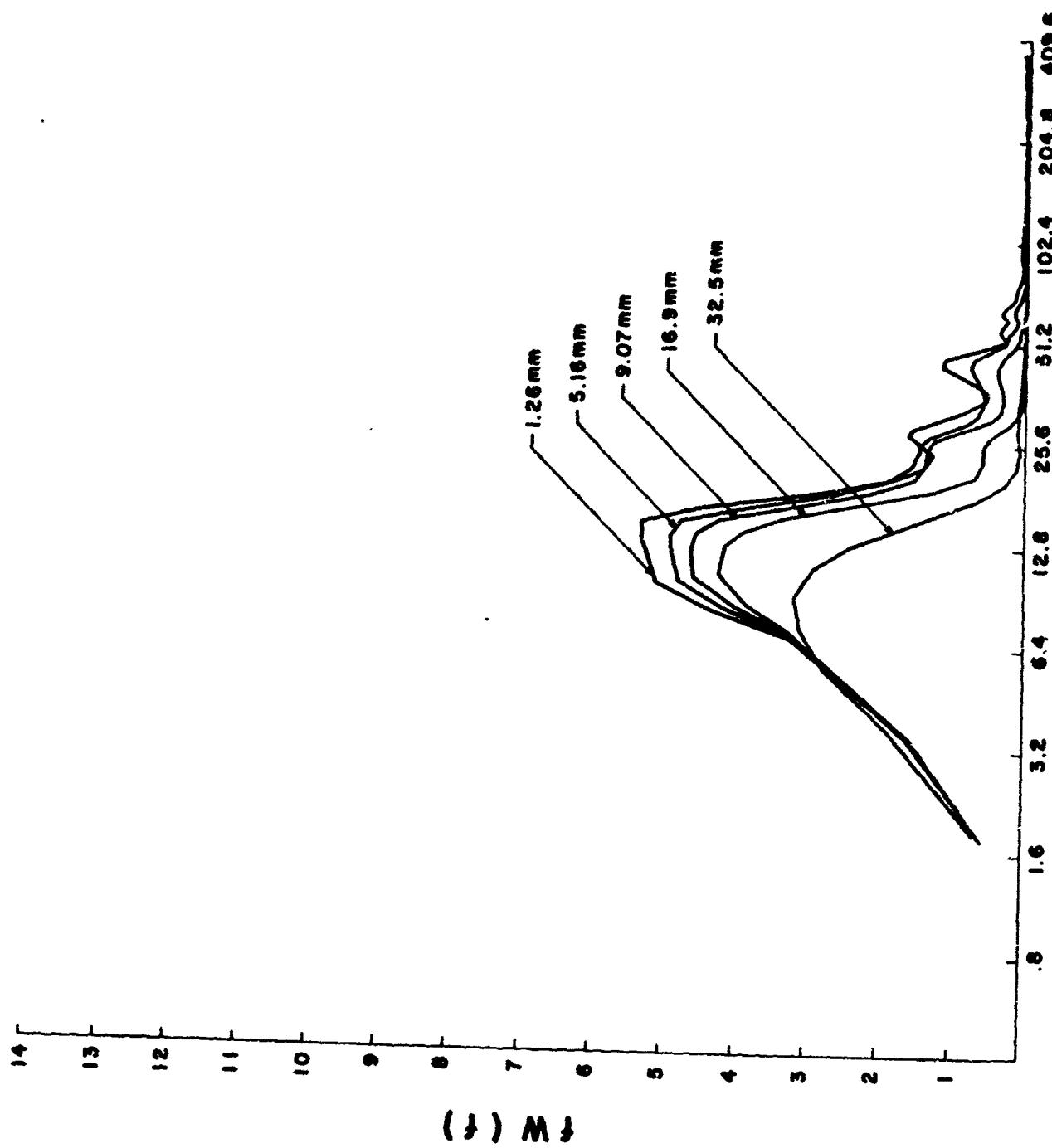
Figure A-20. Spatial frequency times smoothed power density spectrum vs spatial frequency for a series of increasing one-dimensional apertures from afternoon horizontal intensity scan.

Figure A-21. Distribution curve for afternoon horizontal intensity scan
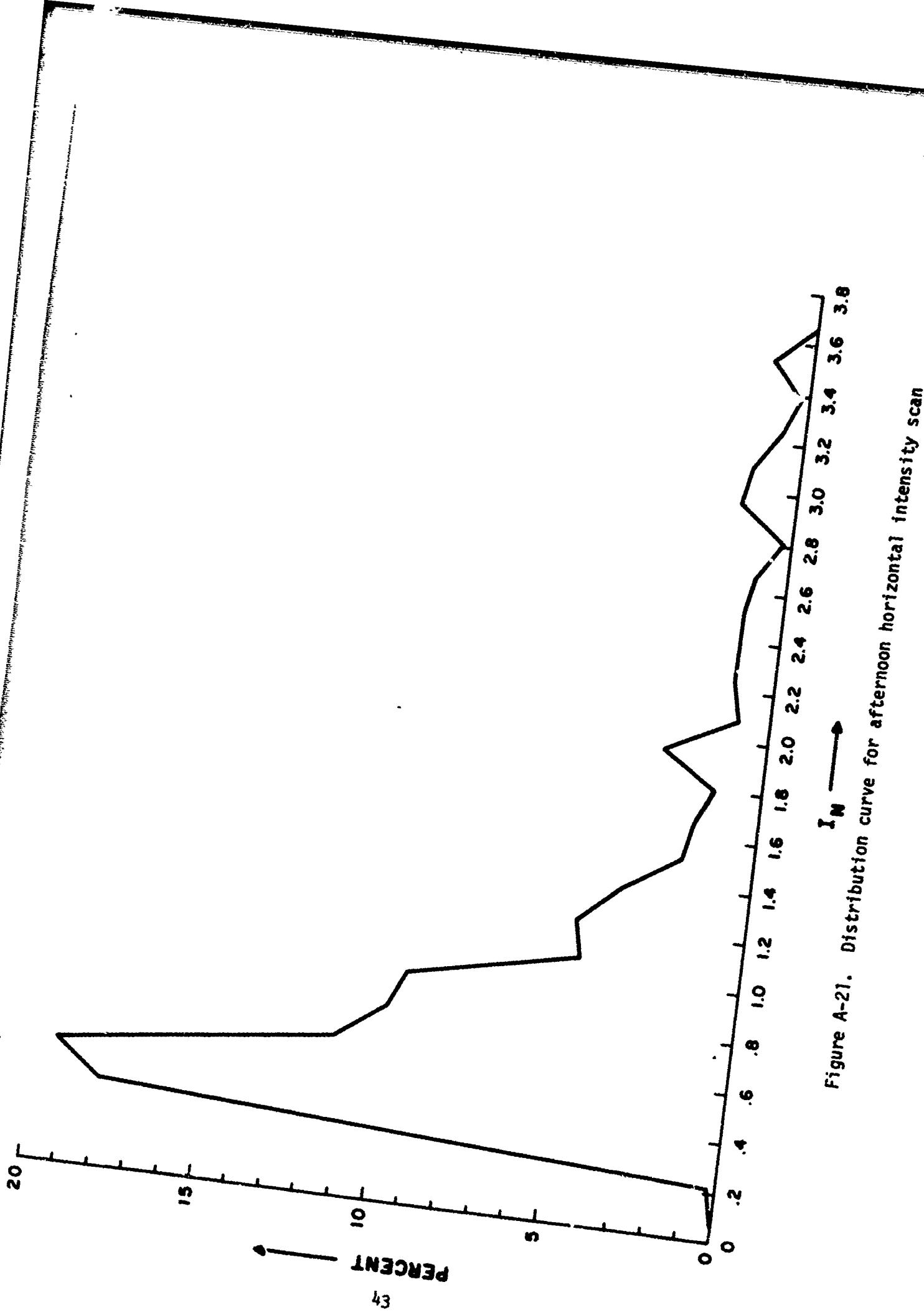
43
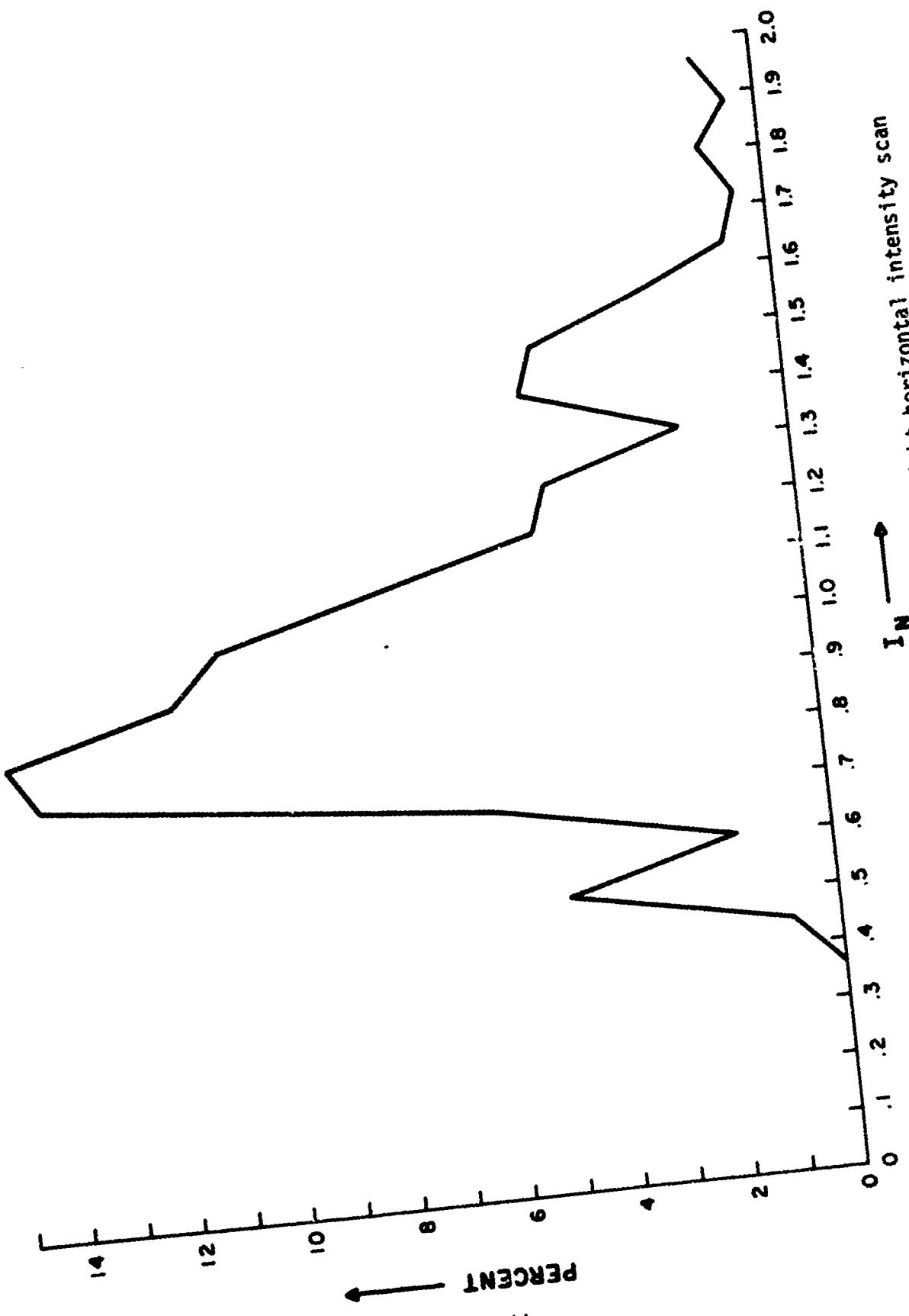
Figure A-22.   Distribution curve for night horizontal intensity scan

44
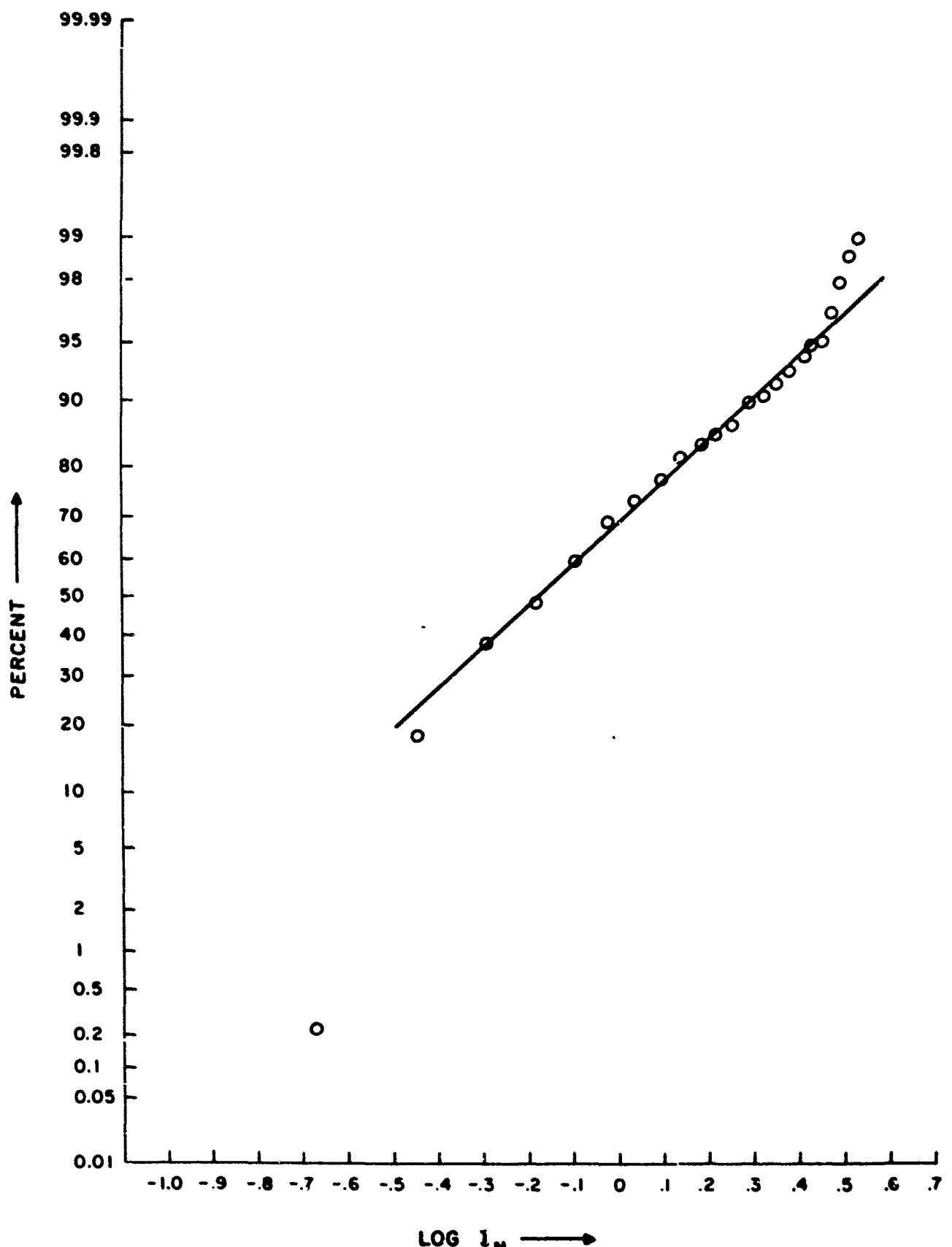
Figure A-23. Cumulative distribution curve for afternoon horizontal intensity scan 45
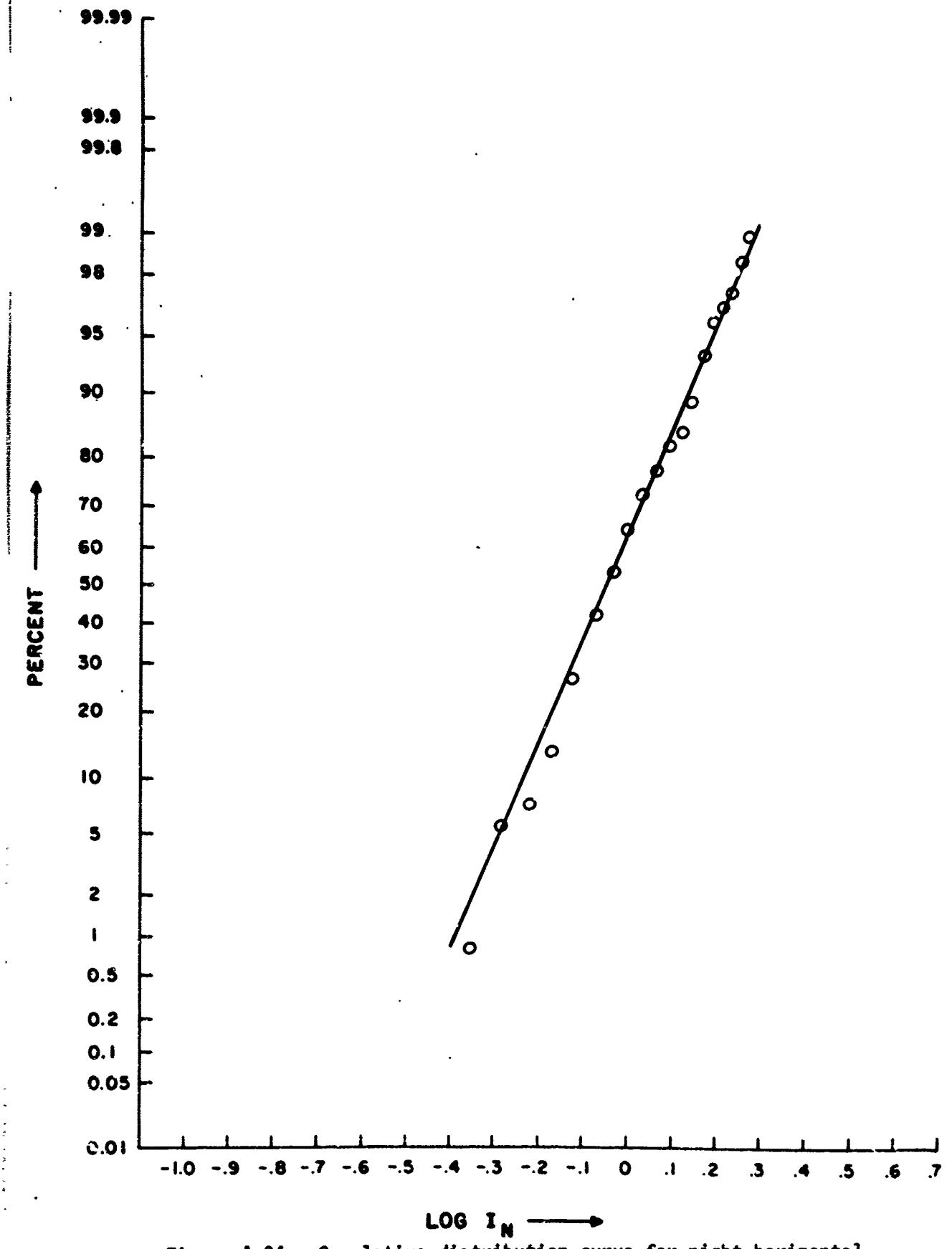
Figure A-24. Cumulative distribution curve for night horizontal
intensity scan   46

DOCUMENT CONTROL DATA - R & D

(Security classification of title, body of abstract and indexing annotation must be entered when the overall report is classified)

1. ORIGINATING ACTIVITY (Corporate author)	2a. REPORT SECURITY CLASSIFICATION
U.S. Army Ballistic Research Laboratories Aberdeen Proving Ground, Maryland	Unclassified
	2b. GROUP

3. REPORT TITLE

OPTICAL METHOD FOR ANALYSIS OF ATMOSPHERIC EFFECTS ON LASER BEAMS

4. DESCRIPTIVE NOTES (Type of report and inclusive dates)

5. AUTHOR(S) (First name, middle initial, last name)

Paul H. Deitz

6. REPORT DATE	7a. TOTAL NO. OF PAGES	7b. NO. OF REFS
July 1967	60	3
8a. CONTRACT OR GRANT NO.	9a. ORIGINATOR'S REPORT NUMBER(S)	
b. PROJECT NO. RDT&E 1P523801A286	Memorandum Report No. 1840	
c.	9b. OTHER REPORT NO(S) (Any other numbers that may be assigned this report)	
d.		

10. DISTRIBUTION STATEMENT

Distribution of this document is unlimited.

11. SUPPLEMENTARY NOTES This material was presented at the Symposium on "Modern Optics," sponsored by Brooklyn Polytechnic Institute and held at Waldorf-Astoria Hotel, New York City, 21-24 March 1967.	12. SPONSORING MILITARY ACTIVITY U.S. Army Materiel Command Washington, D.C.

13. ABSTRACT

This report describes the design of an instrumentation system for the study of the effects of atmospheric turbulence on a collimated laser beam under near-earth conditions.

The instrumentation consists of a helium-neon laser with optical collimator and a receiving system of 24-inch aperture with narrow bandpass filter.

The Appendix presents examples of beam cross section patterns for different propagation conditions. The method of analyzing spatial intensity distributions of these patterns is described.

14. KEY WORDS	LINK A		LINK B		LINK C	
	ROLE	WT	ROLE	WT	ROLE	WT
Laser Propagation						
Atmospheric Turbulence						
Missile Guidance						
Communications						